DESIGN AND PROTOYPING OF A MECHATRONIC SYSTEM AS A DRAG REDUCTION DEVICE FOR BUSSES

A Thesis Submitted to
the Graduate School of Engineering and Sciences of
İzmir Institute of Technology
in Partial Fulfillment of the Requirements for the Degree of

MASTER OF SCIENCE

in Mechanical Engineering

by
Gökhan KAVADAR

June 2006
İZMİR

We approve the thesis of **Gökhan KAVADAR**

Date of Signature

……. **14 June 2006**
Asst. Prof. Dr. Emin Faruk KEÇECİ
Supervisor
Department of Mechanical Engineering
İzmir Institute of Technology

……. **14 June 2006**
Asst. Prof. Dr. H. Seçil ALTUNDAĞ ARTEM
Department of Mechanical Engineering
İzmir Institute of Technology

……. **14 June 2006**
Assoc. Prof. Dr. Salih Okur
Department of Physics
İzmir Institute of Technology

……. **14 June 2006**
Assoc. Prof. Dr. Barış ÖZERDEM
Head of Department
İzmir Institute of Technology

……
Assoc. Prof. Dr. Semahat ÖZDEMİR
Head of Graduate School

ACKNOWLEDGEMENTS

In this thesis study I have learned important things about mechatronic systems and the scientific research process. I would deeply thank my supervisor, Dr. Emin Faruk Keçeci, for giving me the opportunity to work with him in this project. I also want to mention that, apart from the technical lessons, he also gave us important advices which I think are very important for our life.

In addition I also want to thank my family and my best friend for supporting me in this project and giving me the energy to carry on.

This thesis study is supported by İzmir Institute of Technology under the project number IYTE 049 (2005).

ABSTRACT

DESIGN AND PROTOTYPING OF A MECHATRONIC SYSTEM AS A DRAG REDUCTION DEVICE FOR BUSSES

In this thesis study it is intended to design a mechatronic device which will act as a drag reducer for busses. The drag reduction device will be a self operating system, which will be attached onto the front side of the bus. Since the device will operate at the front of the vehicle, it will reduce the front drag force. The mechatronic drag reduction device will have two states; these are the open and close states. Therefore, the device will operate only when it is necessary to operate. That is, normally when the drag force experienced by the vehicle is not at important levels, then the device will stay closed. In the closed position the device will occupy the least space so that it does not cause any difficulties for the driver. However, when the drag force increases, then the device opens and builds itself on the front of the vehicle. The basic idea behind this device is to produce an extra volume of mass at the front of the bus, which will change the incoming airflow, so that the least resistance is experienced by the bus. By reducing the drag force a corresponding amount of fuel saving could be achieved.

The mechatronic device design is made by parametric solid modeling software SolidWorks. The shape of the mechatronic device and the mechanism design will all be made in computer environment. The fluid flow analyses will be also made by using an Engineering fluid dynamics software program called Cosmos FloWorks. The most efficient shape for the mechatronic drag reduction device will be designed by the computer software.

In the scope of this project a small low-speed wind tunnel will be constructed. Besides the virtual analyses made with computer software, real flow tests will be carried out by using a 1:50 scale model bus, attached with a model of the mechatronic drag reduction device. In the wind tunnel tests, the relative reduction in drag forces will be investigated.

ÖZET

OTOBÜSLER İÇİN TEPKİ KUVVETİNİ AZALTACAK MEKATRONİK SİSTEM TASARIMI VE PROTOTİP İMALATI

Bu tez çalışmasının amacı otobüsler için rüzgar tepki kuvvetini azaltacak mekatronik bir burun tasarımıdır. Tasarlanacak olan burun kendin kendine çalışabilme fonksiyonuna sahip akıllı bir sistem olacaktır. Mekatronik burun otobüsün on tarafına monte edilecektir ve bu alanda oluşan tepki kuvvetini azaltmaya yönelik çalışacaktır. Sistemin iki konumu olacaktır, bunlar açık ve kapalı konumlarıdır. Eğer otobüse etkiyen direnç kuvveti az ise o zaman sistemin açık olmasına gerek yoktur ve kapalı duracaktır. Kapalı halde iken sistem en az hacmi kaplayacak şekilde ve otobüsün sürüşünde bir engel teşkil etmeyecek şekilde bir hal alacaktır. Ancak otobüse etkiyen direnç kuvveti arttığı zaman, mekatronik burun açılacak ve otobüsün ön tarafında belli bir şekli oluşturacaktır. Burun sahip olduğu şekil itibariyle otobüse çarpan hava akımının yönünü değiştirecektir ve böylelikle havanın karşı koyma kuvvetini azaltacaktır.

Mekatronik burnun tasarımı bir parametrik katı modelleme programı olan SolidWorks kullanılarak yapılacaktır. Her bir parçanın tasarımı ve bütün olarak mekanizmanın çalışması bu sayede belirlenecektir. Sistemin simülasyonu ise bir akışkanlar mekaniği simülasyon programı olan Cosmos FloWorks kullanılarak yapılacaktır. Bu şekilde otobüse etkiyen direnç kuvvetini en etkili şekilde azaltan burun şekli belirlenecektir.

Bu tez projesi çerçevesinde ufak çaplı bir düşük hızlı rüzgar tüneli imal edilecektir. Bilgisayarda yapılan analizlerin yanı sıra bu tünel kullanılarak 1:50 oranında küçültülmüş bir otobüs modeli üzerinde mekatronik burnun testi yapılacaktır.

TABLE OF CONTENTS

APPENDICES

LIST OF FIGURES

LIST OF TABLES

CHAPTER 1

INTRODUCTION

This research intends to develop a mechatronic device which will serve as a drag reducer. The device is designed for a typical commercial travel bus however; the proposed methods and the device with slight modifications can be applied to other heavy duty vehicles. The device focuses on the front drag force reduction. It consists of mechanical and electronical parts. Due to the mechanical parts, which together make up a mechanical system, the device will be able to open and close itself. That is, the device will have two states, ON and OFF. From this point of view it can be said that the device is an active drag reduction element. The operation principle of the device is to simply alter the shape of the vehicle in order to affect the airflow. By providing a more streamlined flow and preventing pressure increases, the total drag force affecting the vehicle will be reduced. Because this device utilizes an electronic logic circuit, the device itself will be able to decide whether to open or close. In other words, if the vehicle experiences a high drag force, the device will open in order to reduce it.

In the following chapter; basic knowledge on aerodynamic drag force is given and then related background information on the drag reduction concept is presented. Later the design and simulation of the mechatronic drag reduction device in a computer environment is given. Afterwards; the mechanical and electronical part designs are presented. Finally; conclusions of the achieved results and future research opportunities are proposed.

1.1. The Definition of Drag Force

The term “Drag Force” can be broadly defined as the mechanical force which is created when a solid object moves inside a fluid. The drag force is a vectoral force, which means that it has both a magnitude and a direction. When an object moves through a medium, whether liquid or gas, the drag force is acting in the direction opposite to the direction of motion. In other words, the drag force is a resistive force, which prevents or makes the motion difficult. Therefore gaining insight into the nature

of drag force is very important subject in vehicle design. No matter if it is a ground vehicle like automobiles and trucks, or a sea vehicle like ships and boats, or air vehicles like planes and jet fighters; the existence of drag force applies to almost any kind of moving vehicle.

Drag force can be roughly divided into four major components. These are the Pressure (Form) drag, the Skin (Friction) drag, the Induced drag and the Parasite drag.

1.1.1. The Pressure (Form) Drag

The Pressure drag, or also called as Form drag, is a shape depending drag force. This means that if the object has a quite complex shape with sharp corners and quick directional changes in the body contour, then the fluid flowing around it can not adapt itself to these geometrical changes and starts to separate from the surface of the object. When this happens the local properties of the air, like velocity and pressure will vary around the object. This varying pressure distribution will change the momentum of the gas molecules and due to the momentum change a force will be produced. This force is called as the Pressure Drag Force. Pressure drag is mostly occurring at the front and back of the vehicle (Fig. 1.1). At the front of the vehicle a pressure increase is observed, which is called as the *Fore body Drag or Front Drag*. Whereas at the back of the vehicle a pressure decrease, which is mostly the case, is called as the *Base Drag*.

Figure 1.1. Sources of drag for a semi-trailer

(Source: Web_1,2005)

1.1.2. The Skin (Friction) Drag

As the name already implies, the skin drag is related with the surface properties of the object. Technically, when the body moves inside the fluid, it has a boundary layer containing fluid particles moving at the same speed. Since the surrounding fluid is stationary, some amount of energy is required to accelerate the fluid particles in contact with the object surface. This required energy depends on the physical properties between the fluid and the object. For example, for an object which has a very smooth surface with very low friction constant, the generated skin friction drag force will be low. However, for an object with a rough surface and high friction constant, the occurring drag force will be much higher. Therefore, almost any type of vehicle, including airplanes and ships, is specially coated with certain chemicals in order to reduce the skin friction drag force.

1.1.3. The Induced Drag

Similar to the pressure drag force, the induced drag force is also a shape related drag force. The difference of the object's shape causes the flow to have different paths above and below the object, resulting in a pressure difference. The induced drag force is produced this way, which is also called as the drag force due to lift. This type of drag force is especially important in the wing design for air planes. However, this type of drag force also becomes critical for F1 racing cars, where the induced force can become large enough to lift the vehicle.

1.1.4. The Parasite Drag

Apart from the other drag components, the parasite drag is not a shape related drag force. Mainly the parasite drag is the collection of all other drag sources caused by any apparatus or system belonging to the object. Such as the drag forces produced by wing mirrors, windshield sweepers, wheels, ventilation and all other things can be examples of parasite drag.

Table 1.1. Drag levels for commercial vehicles and busses

(Source: Web_2, 2005)

	Commercial Vehicles	Busses
Skin Friction	5%	7%
Fore Body	20%	25%
Underbody (Induced)	50%	30%
Base	25%	38%

1.2. The Determination of Drag Force

All the different components of drag force combine and build a total drag force which is affecting the object. There exists a mathematical expression which is used to determine the drag force acting on a moving object. This is called as the Drag Force Formula and can be expressed as below.

$$F_D = \frac{1}{2} \times V^2 \times A \times \rho \times C_D \tag{1.1}$$

As it can be clearly seen from equation (1.1), the overall drag force (F_D), depends on several parameters. It is directly proportional with the square of the objects speed (V^2). This shows how sensitive the drag force is to an increase in speed. The drag force is also directly proportional to the largest cross sectional area of the object (A), along the direction of motion. Two objects with identical shape but of different size would experience different drag forces. The one with the larger area would experience more drag force then the smaller one. The drag force is also directly proportional with the viscosity of the fluid (ρ), that the object is moving in. That is, the more viscous the fluid, the more force it exerts on the object. If two identical objects would move at the same speed, one in water and one in air, the one moving in water would be subject to a larger drag force. Maybe the most important parameter that the drag force directly depends on is the Coefficient of drag (C_D). The higher the value of coefficient of drag, then the higher drag forces the object experiences.

The coefficient of drag value is a specific parameter for each different type of object and shape (Table 1.2). Since there is not much chance to reduce the drag force by changing the first three parameters of equation (1.1), the best way left is to reduce the coefficient of drag value of the objects. Therefore, the common goal for vehicle designers is to keep the coefficient of drag value for the new designs as low as possible in order to reduce the drag force.

Table 1.2. C_D values for different objects

(Source: Web_2, 2005)

Type of Object	Coefficient of Drag, C_D
Rough Sphere	0.40
Smooth Sphere	0.10
Hollow semi-sphere opposite stream	1.42
Hollow semi-sphere facing stream	0.38
Hollow semi-cylinder opposite stream	1.20
Hollow semi-cylinder facing stream	2.30
Open Wheel, rotating, h/D=0.28	0.58
Squared flat plate at 90°	1.17
Sports Car	0.3 -0.4
Economy Car	0.4 -0.5
Tractor-Trailer	0.7-0.9
Man (upright position)	1.0 - 1.3
Parachutist	1.0 - 1.4
VW Polo (class A)	0.37
BMW 520i (class D)	0.31

1.3. The Importance of Drag Force Reduction

The drag force is affecting many different areas, such as the transportation area or the industrial area. However, it is obvious that the most sensitive area to drag force is the transportation area. The dominant transportation sector, which is affected by drag force, is the ground vehicles. Therefore, the economic improvements and success of

these areas are greatly dependent on the drag force. Data shows that the energy use of ground vehicles is six times larger than both the energy use of aircraft and watercraft in the US (Wood, 2004). A review shows that the ground vehicles use approximately 50% of their total energy to overcome drag force, whereas air and water vehicles use 90% of their energy. Further analysis shows that the total drag of ground vehicles is comprised of 20% skin friction drag and 80% pressure drag (Wood, 2004). A review (Fig. 1.2) of the energy consumption of ground vehicles within the US shows that the energy demands of automobiles stay constant whereas the energy demands of light and heavy duty vehicles increase. From this point of view it is very important to realize that small contributions to drag reduction could turn into big economical success.

Drag force is not only affecting road vehicles, but also sea and aircraft are subject to drag forces. Designers in these areas are constantly searching for better designs which will provide less drag forces.

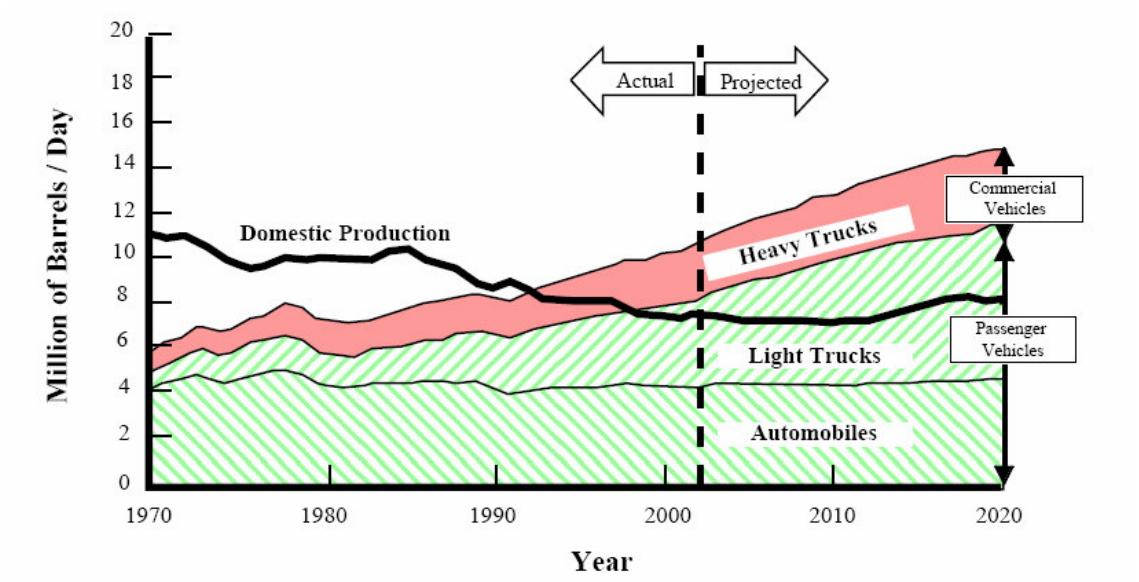

Figure 1.2. A review of energy consumption of ground vehicles

(Source: Wood, 2004)

1.3.1. Drag Force Reduction in Sea Vehicles

Boats and ships are the very early transportation means that humans used to transport both passengers and other goods. In today's transportation area, sea transportation still covers an important portion. Since the drag force is directly proportional with the viscosity of the fluid, the drag forces in water will be higher when

compared with the air. Therefore ships with reduced drag force have become an important point in ship design. In fact, one of the first attempts to improve ship design came from the Vikings. The Vikings started to make their ships taller and with smaller hulls than their counterparts. This design revision enabled them to achieve higher speeds in the seas which provided them an important power. Since then, in maritime technology, engineers and designers are seeking for better hull designs which will have less resistance to the water flow around it. Some examples of new hull designs are the Multihull, Slender monohull and the Semi planning monohull. The multihull design has a smaller surface area, lower weight and as a result experiences less drag than any other hull form. On the other hand, the slender monohull design is narrow and light. It operates with minimum pressure drag but provides limited buoyancy and stability. Next, the semi planning monohull design has a deep v-shaped bow to cut through the waves and a wide shallow rear with a concave or slightly hollow profile under water. Generally in most ship hull designs an artificial nose called as a “bubble” are placed at the front of the ship (Fig. 1.3). The purpose of this part is to divide the water line so that less drag resistance is produced by the water on the ship. Furthermore, some other sophisticated methods, like using gas turbines and water jets in ships are used in order to improve ship design. Also, in ship technology the material selection for the outer part of the ship, which stays in contact with the water, becomes important. The friction drag between the ship and the water is also an important source for drag. Especially algae’s or other factors like corrosion on the hull surface can cause the friction drag to dramatically increase. Therefore special materials and coatings are used to provide a long lasting low friction surface.

The same facts are also applied to underwater vehicles, especially U-boots. Since U-Boots are generally underwater and their entire outer surface is subject to sea water, the importance of the outer material and coating has primary importance. Another important point is the body shape of these vehicles. It is obvious that almost any type of U-Boot has a similar shape, which is like a longitudinally stretched tear drop. The reason for this situation is that aerodynamically the tear drop shape has the lowest coefficient of drag parameter. This means that, it shows the least resistance to the flow. Therefore if there are no restrictions related with the shape, designers tend to liken the shape of their designs to the tear drop shape.

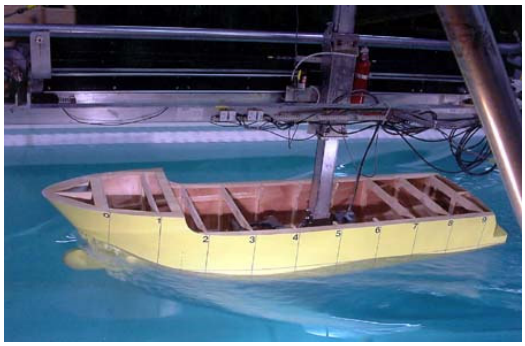

Figure 1.3. Ship hull design tests in a water tank

(Source: Web_7,2005)

1.3.2. Drag Force Reduction in Air Vehicles

In aircraft design, drag force has been always an important design consideration. Since the drag force is directly proportional to the square of the speed of the object, the drag forces related with very high speeds become extremely important. Like it was the case in U-Boots, airplanes also have broadly similar shapes which also resemble the basic tear drop shape (Fig. 1.4). Such design of air planes has greatly reduced the pressure drag force, but due to the very high operating speeds, planes are still greatly – effected by skin friction drag. For modern aircraft, the skin friction drag accounts for more than half of the total drag, therefore more sophisticated methods are proposed to reduce this drag force. Some of the methods include; producing extra plasma fields, vibration, using actuators, flow additives (micro bubbles, polymers and surfactants), flow ribblets, flow blowing or suction in the boundary layer, injection of gases viscosity or different temperature and active boundary layer heating.

Figure 1.4. Commercial type air plane

(Source: Web_8, 2005)

1.3.3. Drag Force Reduction in Ground Vehicles

At the very early times when the automobile technology was not that developed and cars could not reach high speeds, the concept of drag force was not that important for automobile makers and designers. As manufacturing technologies improved and knowledge increased, automobiles and other vehicles like busses and trucks also started to improve. For example, they were able to reach higher speeds. However, the drawback of these technological advances was that, better vehicles with higher performance consumed more energy and this energy was provided by fuel. Sooner or later the concept or fuel efficiency started to became one of the important design issues in vehicle design. Designers started to make more fuel efficient vehicles. At that time the aerodynamic properties of the car started to play an important role in designing the shape of the vehicles. The goal was to design vehicles with lower resistance to airflow. This, in other words, was to reduce the drag force on vehicles, and it was accomplished by changing the body shapes of the vehicles. Also, their goal was to reduce the coefficient of drag of the vehicles. The progress in vehicle design can be easily seen when looking at the early automobile designs and how they evolved (Fig. 1.5). When looking closely, it can be noticed that the early automobiles had too many sharp corners and edges. In later designs, these straight edges and corners started to became smoother and rounder. Each new design shows a dramatical decrease in the coefficient of drag value. Still today every year vehicle manufacturers bring out newer vehicles to the market, which have very different design concepts in comparison to previous ones. The reason is that achieving a slightly better performance and fuel efficiency could move the manufacturer ahead of its counterparts. From this point of view the development of vehicle technology is a never ending story and especially in these days even small improvements could have significant effects on the market.

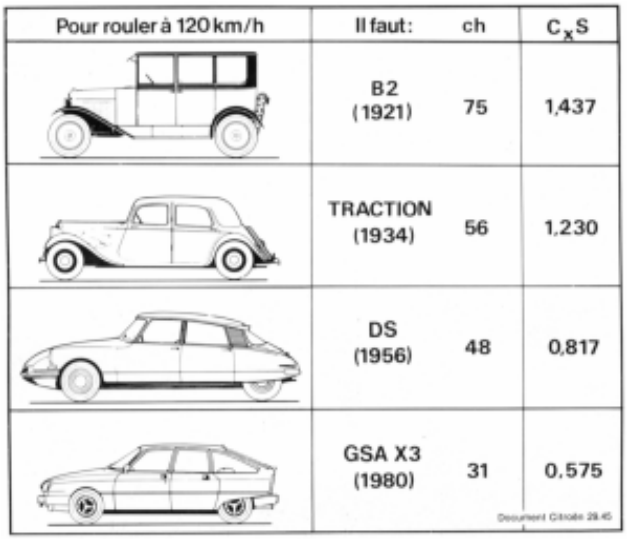

Figure 1.5. Coefficient of drag values of early cars

(Source: Web_3, 2005)

1.4. Previous Works Done in Drag Reduction for Heavy Duty Vehicles

The drag reduction process in fact includes the relative treatments for all of the different drag components, which are mainly the pressure and skin friction drag. However, research data (Wood 2004) shows that the pressure drag component has a much greater effect on the total drag force affecting ground vehicles, therefore more research and proposed drag reducing devices are based on pressure drag reduction. The attempts to reduce the pressure drag force on vehicles can be basically divided into two groups. The first group deals with providing a more attached flow over the vehicle, whereas the second group is focusing on separating the flow (Wood 2004).

The concept of vehicle design with a more attached flow profile is rather old technology. As stated above, the examples of this development process can be found in each different area of transportation vehicles. The attached flow technologies include smoothing out the edges and corners of the vehicles to provide a more streamlined shape. Throughout the years both heavy duty vehicles like trucks and busses, as well as passenger cars and light weight vehicles have evolved from a box shaped figure to a more curved shape with smoother contours and better aerodynamic properties (Fig. 1.6). This type of vehicle shaping has provided drag reduction rates up to 30 %.

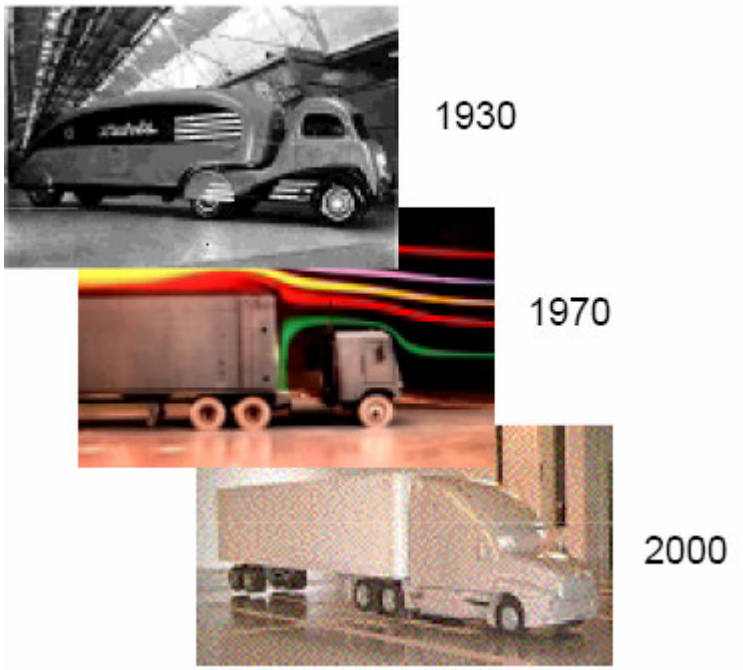

Figure 1.6. Change in shape for heavy duty vehicles
(Source: Wood, 2004)

Compared with the attached flow technology, the separated flow technology is a rather new concept. The basic idea of this technology is to alter the flow field around the vehicle in order to control the airflow and hence reduce the high pressure differences. The first attempts in this area were made by Mason and Beebe (Mason and Bebe 1978) from General Motors. They tested different add on devices in order to reduce the base drag of a tractor trailer (Fig. 1.7). The devices they tested were guide vanes, vertical and horizontal splitter plates and non ventilated cavity. The experiments showed that only the non ventilated cavity design, which in fact are plates attached at the back of the trailer, had significant effects on drag reduction. By varying the depths of the plates, they concluded that the optimum plate length is 0.13d, where d stands for the height of the trailer. The result was a 5% of drag reduction for a 48 foot trailer. In fact the concept of base plates has its origins in aircraft technology, where Bearmann (Bearmann 1965, Bearmann 1966) in 1966 applied this technology to reduce the base drag of blunt trailing edge airflows and achieved a 10% drag reduction.

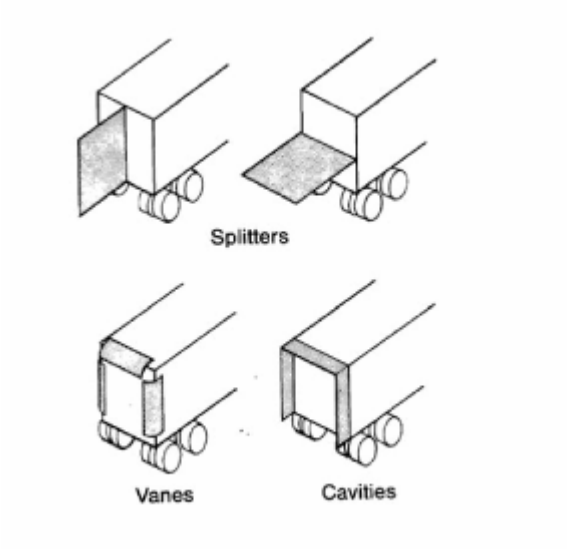

Figure 1.7. Mason and Beebe's add on devices

(Source: Mason and Bebe, 1978)

Later in the 1970's the same technology of base plates was tested by Hucho on smaller mini van style vehicles. From his experiments he showed that the result coincides with the previous results in reference (Mason and Bebe 1978). The same technology was further investigated in 1988 at the NASA Ames Research Center. This time researchers moved the base plates to an inset from the perimeter of the trailer (Fig. 1.8). In this approach the optimum plate length is found to be 0.36w at an inset of 0.06w, where w represents the width of the trailer. From the experiments it is concluded that for a 48 foot trailer a drag reduction of 10% could be achieved over a ±15º yaw angle range.

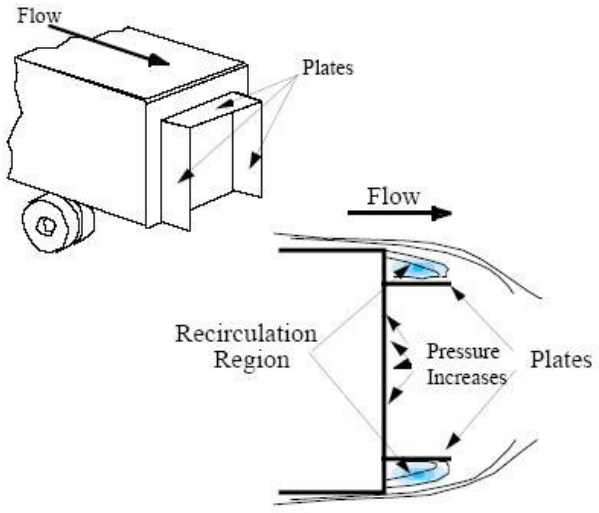

Figure 1.8. Base plates attached to the back of a trailer

(Source: Wood, 2004)

An important source of drag for a typical tractor trailer combination is the gap between the tractor and the trailer. Various researches have been made to understand how the gap size affects the total drag force (Wood and Bauer 2003). Results show that reducing the length of the gap has positive effects on drag reduction, also blocking and sealing the gap greatly reduces the drag force. Wood and Bauer (Wood and Bauer 2003) proposed an aerodynamic device which is called as the *Cross Flow Vortex Trap Gap*. Initially the concept of vortex traps were developed for aircraft, that is for various airfoils and three dimensional wings, by Kasper (Kruppa 1977). Wood and Bauer applied this technology to ground vehicles by attaching plates vertically to the front face of the trailer (Fig. 1.9). When the airflow enters the gap, it starts to form turbulence and increase the drag force. However, when the plates are present, the air streams are individually trapped between the plates and prevented from forming into a large turbulence, hence decreasing the total drag. A drag reduction up to 30% is claimed to be achieved by this way.

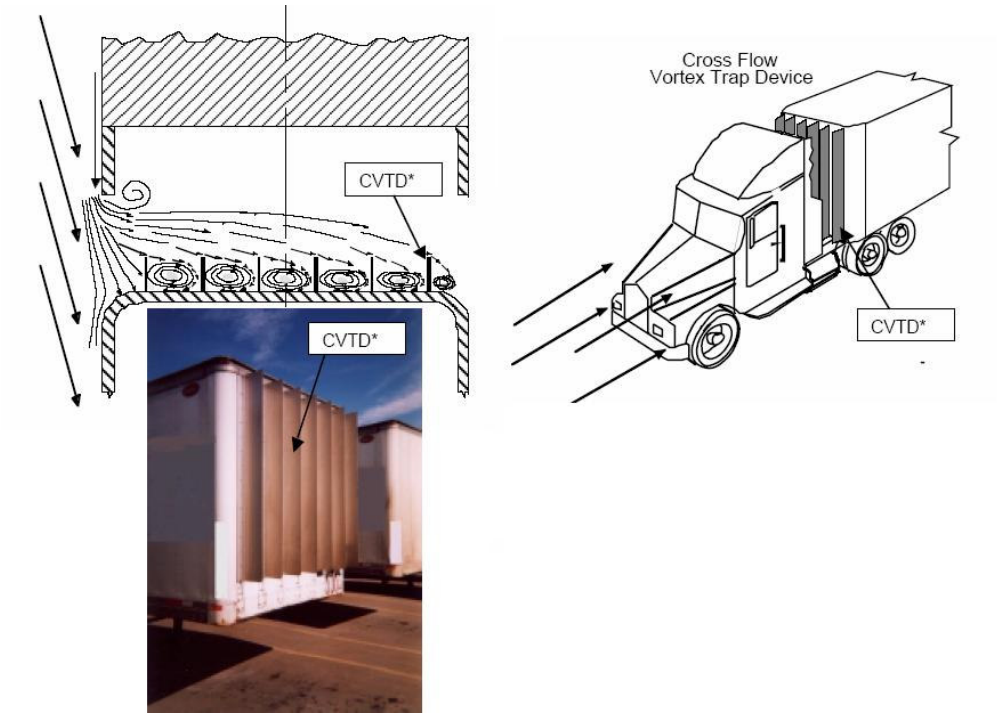

Figure 1.9. Cross flow vortex trap gap device
(Source: Wood and Bauer, 2003)

Another important achievement in drag reduction technology was developed by Englar (Englar 2001). Englar transferred the existing pneumatic aircraft technology to heavy duty ground vehicles. The pneumatic aerodynamic device consists of blowing air

into the boundary layer of the free stream (Fig. 1.10) and thereby increasing the momentum of the air. Blowing slots on both the leading edge and the trailing edge can provide a drag reduction rate about 50% when blowing with 1 psig blowing pressure. Tests showed that by increasing the blowing rate of the air, an 84% drag reduction could be achieved.

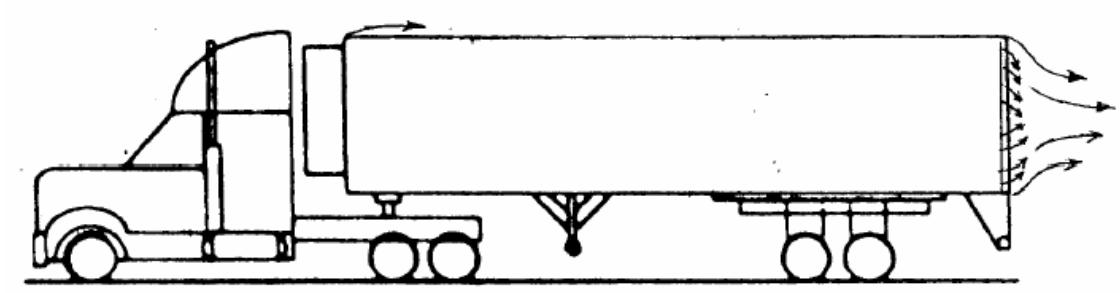

Figure 1.10. Schematic of pneumatic aerodynamic technology applied to heavy vehicle trailer (Source: Englar, 2001)

A similar device to Englar's was developed by Modi (Mode and Desphonde 2001) who also applied the same principle from aircraft technology to ground vehicles. Modi used the Moving Surface Boundary Layer concept as a template and tested the use of rolling cylinders as moving surfaces (Fig. 1.11). The rotating cylinders add momentum to the airflow and thus provide a more controlled flow around the vehicle. A Drag Reduction of 30 % has been reported by this study.

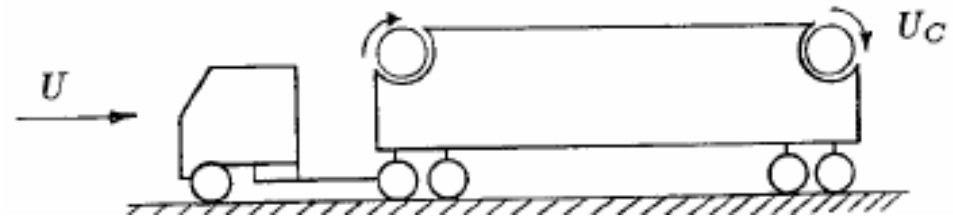

Figure 1.11. Schematic of rotating cylinder applied to heavy vehicle trailer (Source: Mode and Desphonde, 2001)

A different approach was proposed by Wood and Bauer (Wood and Bauer 2001, Wood and Bauer 2003), which initially was used in the industrial area. The device is merely a porous skin which is mounted onto the trailing surface and/or aft portions of the ground vehicle (Fig. 1.12). The porous surface is separated from the surface of the trailer by at least one thickness of the porous skin. The function of the porous surface is

to reduce the flow separation in the base and wake regions, prevent turbulence formation and support the attached flow. Results show that a drag reduction of 15% could be achieved this way.

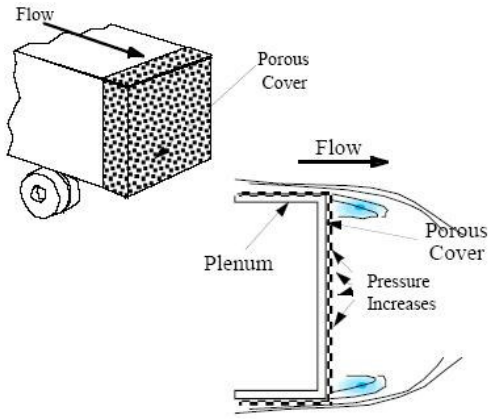

Figure 1.12. Porous surface attached to the rear surfaces of the trailer
(Source: Wood, 2004)

Vortex generators are another type of aerodynamic devices which have been used in aircraft technology. The idea behind vortex generators is to energize the airflow in order to prevent the flow separation and thus reduce drag force. One of the aerodynamic devices based on this principle was proposed by Wood and Bauer (Wood and Bauer 2003), which is called as the *Vortex Strake Trailer Base Treatment Device* (Fig. 1.13). The vortex strakes are installed at the rear surfaces of the trailer to energize the airflow and prevent it from creating turbulence in the wake region of the trailer. It is reported that drag reductions greater than 10% have been achieved with this design.

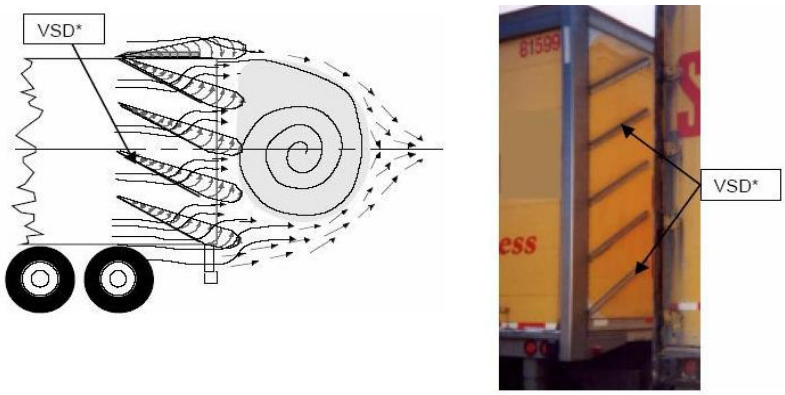

Figure 1.13. Vortex strake trailer base treatment device
(Source: Wood and Bauer, 2003)

A similar device proposed by Wood and Bauer (Wood and Bauer 2003) is the *Undercarriage Flow Treatment Device*. This device is simply a contraction cone design, which adds momentum to the flow coming below the vehicle and directs it with increased velocity into the wake region of the trailer (Fig. 1.14). The basic principle of this aerodynamic device is to prevent or reduce the turbulence formation at the wake region of the trailer. In this design; the shapes of the flaps are important. Tests showed that this device achieved a drag reduction greater than 10%.

Figure 1.14. Undercarriage flow treatment device

(Source: Wood and Bauer, 2003)

CHAPTER 2

ENGINEERING FLUID DYNAMICS

2.1. Introduction to Engineering Fluid Dynamics (EFD)

Cosmos FloWorks belongs to a new generation of fluid dynamic simulation software. This new approach amongst simulation software is referred to as "Engineering Fluid Dynamics" (EFD). Despite the fact that both EFD and CFD (Computational Fluid Dynamics) software are based on the same mathematical model, there are some important radical differences between them. The basic differences of EFD software is;

- Integrated with a Solid Modeling Software
- Easy to Use
- Reduced Analysis Time
- Easier Iterative Design Testing

The integration of fluid dynamics software into solid modeling software has brought many advantages over the conventional CFD software. Traditional CFD software are stand alone products which means that the user created geometry must be converted into the proper format to be used with the analysis package. Most of the time the conversion is made in terms of surface data, which generally requires considerable amount of effort and lacks reliability. Small design features in the model, like gaps or small extrusions, are superfluous to the analysis. Due to the integration of EFD software into CAD software, the CAD data of the solid model can be easily transferred to the analysis software without dealing with conversion issues related with the analysis code. Moreover they can automatically detect superfluous features and adapt the analysis to it, resulting in faster calculation time.

As opposed to CFD software, which requires highly trained specialists, EFD programs do not require deep technical knowledge of fluid dynamics concepts. The primary importance of EFD analysis programs is that they are easy to learn. While CFD soft wares require the user to specify specific flow related parameters like relaxation

factors, turbulence transition points or residual requirements, EFD soft wares basically require the engineering goal of the analysis with the desired accuracy. Then the internal solver algorithm automatically specifies the most appropriate parameters for the analysis, such as the mesh generation for the model. The automatic detection of these parameters also leads to a faster convergence of the desired goals which results in shorter calculation times.

Generally in engineering design it is essential to improve the design and ask the "what if" questions. According to the analysis results, models are redesigned and tested. In this sense it is important to rapidly adapt existing designs with small modifications into the analysis. The fully integrated EFD software provides a basis for a collaborative design environment.

2.2. Fundamentals of Computational Fluid Dynamics

Basically the term Computational Fluid Dynamics stands for the use of computer power to analyze and solve classic fluid dynamic problems. The most essential consideration in CFD is how each different CFD program approaches the continuous fluid flow problem and solves it with numerical methods on the computer. The general method, which is widely accepted, is to divide the spatial domain into small discrete cells to form a volume mesh. Then an appropriate mathematical algorithm is used to solve the equations of motion that is Euler equations for inviscid flow and Navier-Stokes equations for viscid flow. The mesh generation can be either irregular, which requires that each cell must be stored in memory separately, or regular. In the case of a highly dynamic problem occupying a wide range scale, the mesh generation itself must be modified with time. In this case, adaptive mesh refinement methods are used. Apart from the mesh based method, alternative solution methods exist such as, smoothed particle hydrodynamics, spectral methods and Lattice Boltzmann methods. The first one utilizes a Lagrangian method to solve the fluid problem, whereas the second one is a technique which uses the spherical harmonics and Chebyshev polynomials as a base function to solve the problem. The last one simulates an equivalent mesoscopic system on a Cartesian grid instead of solving the macroscopic system.

The Navier-Stokes equations are used to determine Laminar flow. However; turbulence flow requires a different method because of the range of length scales in turbulent flow. In these cases turbulence models like Large Eddy Simulation (LES) and Reynolds averaged Navier-Stokes (RANS) are used with the k-ε model or the Reynolds stress model. In most cases other equations like heat transfer and chemical reaction are also simultaneously solved.

The basic methodology for typical CFD software is the same, despite their different approach;

1. The geometry of the problem is defined, mostly using CAD tools.
2. The mesh is generated. The fluid volume is divided into discrete cells.
3. Physical modeling is defined, such as conservation laws, motion, etc.
4. Boundary conditions are specified. If required initial conditions are also defined.
5. The equations are solved numerically.
6. Analysis solutions are visually presented.

2.2.1. Mesh Generation Method

Mesh generation or "discretization", is generally made numerically rather than analytically. It is important to ensure that the discretization can handle discontinuous solutions. Some of the methods being used are:

- Finite Volume Method
- Finite Element Method
- Finite Difference Method
- Boundary Element Method

Amongst these methods the first one is the standard approach used in many CFD programs. In this method the governing mathematical equations are independently solved for each discrete control volume. The integral approach in (2.1) is inherently conservative that is, quantities such as density remain physically meaningful.

$$\frac{\partial}{\partial_t}\iiint QdV + \iint FdA = 0 \tag{2.1}$$

Where Q is the vector of conserved variables and F is the vector of fluxes.
The Finite Element Method is generally used for structural analysis of solids, the Finite Difference Method is limited with simple geometries which have regular meshes and in the Boundary Element Method the boundary occupied by the fluid is divided into surface meshes.

2.2.2. Turbulence Models

Turbulent fluid motion is highly random, unsteady and three dimensional. Also, it consists of many eddies with different lengths and time scales. It is believed that the turbulent flow can be exactly described by the Navier-Stokes equation. Tough numerical solutions are available for these equations, the current storage capacity and speed of computers is not sufficient to obtain a solution for a practically relevant flow. This method is known as Direct Numerical Solution (DNS). Since the turbulent flow can not be calculated with an exact method, different methods are used.

- Reynolds averaged Navier-Stokes (RANS)
- Large Eddy Simulation (LES)
- Detached Eddy Simulation (DES)

2.2.2.1. Reynolds Averaged Navier Stokes

In the Reynolds averaged Navier-Stokes (RANS) method is obtained from the Navier-Stokes equations. The Navier-Stokes equations are derived from the basic conservation laws that apply to the motion of a fluid. These are the basically the mass and momentum conservation laws and the viscous effects on the fluids. In the following equations ρ represents the density of the fluid; p is the pressure; ν stands for the kinematic viscosity and $\underline{u}$ is the velocity vector of the fluid.

Conservation of Mass:

$$\frac{\partial \rho}{\partial t} + \nabla \cdot (\rho \underline{u}) = 0 \qquad (2.2)$$

Conservation of Momentum:

$$\frac{\partial \underline{u}}{\partial t} + \underline{u}(\underline{u} \cdot \nabla) + \frac{1}{\rho}\nabla(\rho) = F \tag{2.3}$$

Viscous Effects:

$$F_{Vis} = \nu \nabla^2 \underline{u} \tag{2.4}$$

Finally for incompressible fluids with constant density the Navier-Stokes equation will become;

$$\nabla \cdot \underline{u} = 0$$

$$\frac{\partial \underline{u}}{\partial t} = -\underline{u}(\underline{u} \cdot \nabla) - \frac{1}{\rho}\nabla(p) + \nu \nabla^2 \underline{u} + F \tag{2.5}$$

The Reynolds averaged Navier-Stokes equation is obtained by assuming the physical variables to be composed of mean and fluctuating components, which is known as Reynolds decomposition.

$$u(x, y, z, t) = \bar{u}(x, y, z) + u'(x, y, z, t) \tag{2.6}$$

The mean components are constant over time whereas the fluctuating components vary with time. The fluctuating components are expressed in terms of the mean components and then only the mean components are solved. The resulting solutions describe the mean flow field and introduce an additional unknown called as Reynolds Stress.

$$\begin{aligned} \bar{\tau}_{xx} &= \rho \overline{u_x' u_x'} \\ \bar{\tau}_{xy} &= \rho \overline{u_x' u_y'} \\ \bar{\tau}_{xz} &= \rho \overline{u_x' u_z'} \end{aligned} \tag{2.7}$$

The Reynolds stresses have significant effect on the flow and must be modeled in terms of mean flow quantities.

One of the methods, based on Boussinesq (1877), is the Eddy Viscosity method, assuming that the energy dissipation within the turbulent flow can be modeled by an "eddy viscosity".

$$-\rho u_i' u_j' = \mu_t \left(\frac{\partial \overline{u}_i}{\partial x_j} + \frac{\partial \overline{u}_j}{\partial x_i} \right) - \frac{2}{3} \rho \delta_{ij} k \tag{2.8}$$

Where μ_t is the eddy viscosity and k is the turbulent kinetic energy. The turbulent kinetic energy is defined as;

$$k = \frac{1}{2} u_i' u_i' = \frac{1}{2} (u_x' u_x' + u_y' u_y' + u_z' u_z') \tag{2.9}$$

Dimensional analyses show that the eddy viscosity can be formulated as;

$$\mu_t = C \rho v_T l \tag{2.10}$$

Where C is a dimensionless constant, v_T is the velocity scale and l is the length scale.

Another method is the Mixing Length Model proposed by Prandtl. In this model the eddy viscosity is defined by;

$$\mu_t = C \rho l k^{1/2} \tag{2.11}$$

The turbulent kinetic energy, k, is commonly determined by the k-ε model. This model relates the eddy viscosity to the turbulent kinetic energy, k, and the turbulent dissipation rate, ε. The model is also called a two equation model, because it requires an additional partial differential equation to incorporate the turbulent dissipation rate.

$$\mu_t = \frac{C \rho k^{1/2}}{\varepsilon} \tag{2.12}$$

Other methods derived from the k-ε model are the RNG k-ε method, in which k-ε are derived from a statistical technique known as Renormalization Group Method. The RNG k-ε model has improved predictions in transitional flows, wall heat and mass transfer and high streamline curvature and strain rate. Another method is the k-ε

realizable model which uses a variable C_μ instead of constant. This model has improved performance in planar and round jets, rotation, boundary layers with strong separation and strong streamline curvature.

In cases where flow separation is important, the k-ω method is used. The k-ω model is also a two equation model and thus requires two additional partial differential equations: one for the modified k equation of the k-ε model and one for the ω transport equation. In this model ω is an inverse time scale that is associated with the turbulence. The turbulent viscosity is expressed as follows;

$$\mu_t = \frac{C\rho k}{\omega} \tag{2.13}$$

Another model is the Spalart-Allmaras one equation model. This model solves one conservation equation and is developed for use in unstructured codes in aerospace industry. This shows good performance in attached-wall bounded flows and flows with mild separation and recirculation. However it is not suitable for massively separated flows, free shear flows and decaying turbulence.

The Reynolds Stress model is also called the seven equation model and uses additional transport equations for the six independent Reynolds stresses. This model is especially good in predicting complex flows including cyclone flows, swirling combustor flows and flows involving separation.

2.2.2.2. Large Eddy Simulation (LES)

The Large Eddy Simulation is a technique in which the large scale motions of the flow are calculated. The smaller motions are filtered and modeled using a Sub-grid model. LES can accurately predict the large scale turbulent structures that are most important in the transport quantities. LES requires a more refined mesh than RANS but a coarser mesh than DNS, which places it in between them in terms of computational effort.

2.2.2.3. Detached Eddy Simulation

Detached Eddy Simulation (DES) is a hybrid technique, where LES calculations are carried out in fine regions of RANS model sub-grid scale formulation. DES model provides more numerically feasible and accurate results for massively separated flows.

2.3. Cosmos FloWorks

Cosmos FloWorks uses the Reynolds averaged Navier-Stokes equations along with the k-ε type of turbulence model. The code uses a segregated type solver. The solution scheme for this type of solver is as follows:

1. Firstly, the momentum equations are solved. (u,v,w)
2. The pressure correction equations are solved. To correct fluxes and velocities.
3. Finally, the transport equations for other numbers are solved.

2.4. CFD vs. Wind Tunnel

Engineering problems often require an experimental approach to clearly understand and visualize the problem. Strength analysis and Fluid flow analysis are the most common types of experiments made in engineering science. Today, the developments in computer science make it possible to conduct these experiments entirely in the software environment. There are quite important advantages of the computer simulations against the real experiments. Especially in Fluid Dynamic experiments, there are important differences in performing a Wind Tunnel test and by using Computational Fluid Dynamic programs on the Computer.

Wind tunnel experiments are very expensive processes. Either the designer must build a small scaled wind tunnel which fits his needs, or he must pay for wind tunnels to conduct the experiment. However, by using CFD simulation software, no additional equipment or system is required. One PC with optimum configuration will suffice for the entire analysis of the flow problem. The cost of this will be far cheaper than the real wind tunnel experiment. Another fact is that wind tunnel experiments last longer than CFD simulations. The experimental setup must be prepared certain measurements must be made to be able to get better results from the tests. On the other hand, in CFD

simulation all the detailed adjustments are made by the software itself, and if needed the operator can easily modify them. In virtual simulation the operator has more control over the setup, and can get results from any desired point on the model. In the wind tunnel though, measurement devices must be applied to the points of interest and this brings some limitation to the experiment. In real world experiments, the model has to be scaled according to the properties of the wind tunnel. In the CFD simulation there is no need for such a limitation, the model can be tested at any scale. Another important advantage of CFD simulation is that any experiment can be repeated, however in the real case some experiments can not be repeated, because of economical issues or other problems. Wind tunnel experiments require authorized and specialized personnel. Some type of experiments could be dangerous and special training may required. However with CFD simulation any type of experiment can be safely simulated and no special training is needed. Even newer technologies in CFD software which are called EFD (Engineering Fluid Dynamics) software are simply goal oriented and do not require special knowledge on fluid dynamics.

All these important differences between CFD simulation and real wind tunnel testing clearly show that, use of CFD software is a more efficient way to obtain information on a certain fluid problem. Improved modeling techniques of fluid flow and numerical analyses methods make today CFD programs reliable. Especially for low budget projects or small personal or educational projects it is more preferable to choose CFD simulation. However, it should be taken into account that the wind tunnel tests can provide more realistic results than software simulations. Therefore, it is important that the researcher decides whether it is required to do a wind tunnel test or not. Generally in research projects involving fluid dynamics, it is preferred to use both soft ware simulation and wind tunnels.

CHAPTER 3

THE MECHATRONIC DRAG REDUCTION DEVICE

3.1. The Purpose of the Device

In this project it is aimed to design an aerodynamic drag reduction device for busses. However, the proposed device will also be also easily applicable to other heavy duty vehicles like trucks and tractor trailers. There are basically three important differences of this device which distinguishes it from the previously mentioned aerodynamic drag reducers.

The aerodynamic drag reduction devices which have been developed are basically dealing with the reduction of the base drag and with the gap between the tractor and the trailer. A large portion of those devices are shaping the flow at the rear of the vehicle in order to prevent less turbulence and hence reduce the total drag force acting on the vehicle. The rest of the devices are operating with the same principle and dealing with the turbulence formation inside the gap between the tractor and trailer. Each of those different devices provide different amount of drag reduction. This shows that research on drag force reduction has been mainly focused on base drag reduction. In contrary to those devices, the mechatronic drag reduction device is focusing on the front drag reduction. The front drag and base drag together make up the pressure drag. Data shows that for a commercial bus the base drag is the dominant component (Table 1.1). However, the effect of the front drag can not be ignored. A reduction in the front drag force will also turn into a reduction reduce in the total drag force.

Another important property which the great majority of previous devices in common have is that they are somehow passive devices. By the word “passive” it is meant that, these devices do not have an actively operating mechanism part. Most of them are specially designed plates, stripes or other forms of material. Those types of aerodynamic devices operate on the vehicles until they are removed from the vehicle. Therefore the driver has no control over the devices to let them operate or not. While some of the devices do not affect much the visual appearance of the vehicle, some of them could result in a bad visual appearance. Meanwhile, the mechatronic drag

reduction device unlike previous devices does not alter the overall shape or appearance of any vehicle. As the name of it already implies, this device is in fact a mechatronic system which consists of both mechanical and electronical parts. Due to this mechatronic design, the device has two conditions. These are the ON and OFF positions. This means that, the device is either closed and does not operate, or it is open and operates. The benefit of such a design is that, the vehicle device operates only when it is necessary to operate and the driver can also manually enable or disable the device according to different situations.

It may be noticed that all of the previous research done and the devices proposed are done for trucks and mainly tractor trailers. As it was mentioned previously the energy consumption of light and heavy duty vehicles increases every year. Therefore research has been made on those heavy duty vehicles. However, it should be considered that busses are also a sort of heavy duty vehicle, when classified according to the miles traveled per year. From this point of view, drag reduction research in bus technology is as important as in truck technology. In this project the mechatronic drag reduction device is designed for long distance travel busses. However, the basic concept of the device can be easily adapted to any kind of heavy duty vehicle.

3.2. The Operation Principle

As it was already stated above, the mechatronic drag reduction device is dealing with the front drag reduction of a typical travel bus. Therefore it is going to operate at the front side of the vehicle (Fig. 3.1).

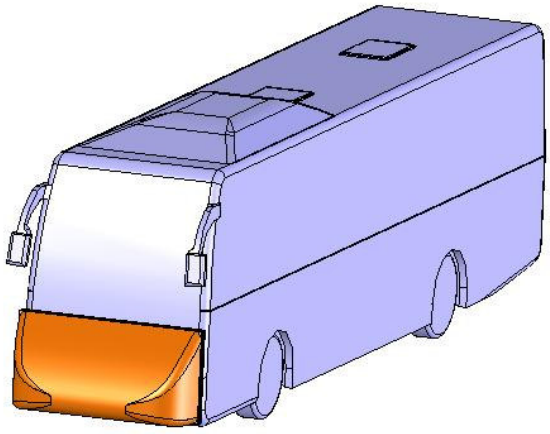

Figure 3.1. The mechatronic drag reduction device

It is important that the vehicle does not cause any restrictions to the drivers viewing range during the trip. To overcome this issue, the device has been designed as a mechatronic system, which means that the device is able to open and close itself. When the vehicle is moving on a highway at 100 km/h then the least distance it should have with the vehicle in the front should be 50 meters. This is a general rule in traffic, which states that the least space which be conserved between two adjacent vehicles is the half of the speed in meters. From this point of view, when the bus is moving with such large speeds on the highway, the device is sitting in the unused area for the driver, which means that it does not cause any complication to the drivers view. Similarly, when the device is in its OFF or closed position it also does not interfere with the drivers view because it changes its shape into a smaller volume and fits into a smaller space (Fig. 3.2).

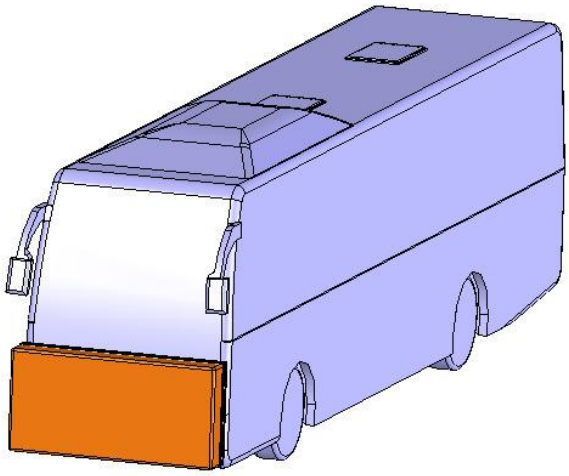

Figure 3.2. The closed position of the device

The operation principle of the mechatronic drag reduction device is basically very similar to the previous introduced devices. In all aerodynamic drag reduction devices, the common operation principle is to affect the flow field around the vehicle. Exactly the same idea holds for the mechatronic drag reduction device. The basic idea is to alter the shape of the vehicle in order to provide a more attached flow around it. To improve the airflow, the device has been designed in a certain geometrical shape. The most important parameter which affects the airflow and the overall drag reduction rate is the geometrical specification of that particular shape. Assume that a bus, without the device installed, is moving on the highway at a speed of 120 km/h. When there is no

wind, the air is assumed to be stationary and the vehicle is penetrating the air at that speed. While the vehicle is moving through the air, it will trap some of the air at its front. Since it will not be easy for the air to escape to the sides because of the geometric front shape of the bus, the pressure in that area will increase. On the other hand, at the back of the vehicle the airflow will produce turbulence and create wake regions, where the pressure will be relatively low. Hence, a drag force dependent on the pressure difference between these two places will be generated. Therefore to achieve a lower drag force, the pressure difference at these places must be kept as low as possible. In the case where the drag reduction device is installed, the frontal shape of the vehicle will change. This deformation in body shape will also influence the airflow around the vehicle. Due to the shape of the device, the airflow coming towards the vehicle is prevented from directly hitting the front of the vehicle. The smoothly curved contours of the device also enable the airflow to easily escape to the sides, so that they do not increase the pressure in that area. In this way, a more attached flow and a more streamlined shape is given to the vehicle. The pressure gradient between the front and rear of the vehicle will be reduced, which also means a reduction in the overall drag force.

As stated above, the mechatronic drag reduction is an active mechanism which is able to close and open itself. There are a couple of benefits this. First of all, in this design the device has two states. Either it is open and operates as a drag reducer, or it is closed. Why this function is important can be easily understood with an example. Assume that a travel bus going from city A to B is traveling on the highway. When the bus is on the highway its speed will be high and automatically the drag force affecting the bus will increase. In this case the driver will want to activate the mechatronic drag reduction device to reduce the experienced drag force and the consumption of fuel. However, to reach city B the bus has to pass through a number of cities, where it must go through the city traffic and obey the speed obligations. Furthermore, if the rush hour city traffic is taken into consideration it is obvious that the bus will move at relatively low speeds and very small distances will be kept between adjacent vehicles. Moreover, in traffic the driver has to be able to do critical maneuvers. Therefore, it makes more sense to disable the drag reduction device so that the vehicle returns to its original state. The mechatronic drag reduction device can either be controlled manually by the driver or the device can automatically decide whether to open or not, based on its electronic logic circuit.

3.3. The Design of the System

The design of the mechatronic drag reduction device has been done in two steps. In the first step, the appropriate shape of the device has been evaluated. Then, in the second step of the design process the mechanical and electronical parts of the system were designed. In this chapter, the evolution of the design process is explained.

In designing the shape of the drag reduction device, the determination of the geometry, which directly affects the drag reduction rate, has become the most important part of the design process. Since the device will directly affect the flow field of the vehicle, a clear understanding must be gained on how different geometric shapes affect the airflow. In order to have wider testing possibilities, the design process was made entirely in a computer environment. The three dimensional model of the bus, is simulated by using SolidWorks™ modeling software. The Wind tunnel analyses are made using a commercial Fluid Dynamics program, called Cosmos™ FloWorks, which is an EFD (Engineering Fluid Dynamics) Software and also a SolidWorks™ plug-in.

The three dimensional model of the bus (Fig 3.3) is modeled in full-scale (1:1) after a MAN Fortuna type model bus (1:50). The detail level for the model is kept at a point between very simple and realistic. A very simple model was not preferred since it would lack some important properties like the side mirrors, air conditioner housings, which in fact have significant influence on the airflow. Therefore a more detailed model was modeled, but also bearing the fact in mind that a too complicated model would require more complex analysis. The following device designs and fluid dynamic analyses are all based on this bus model.

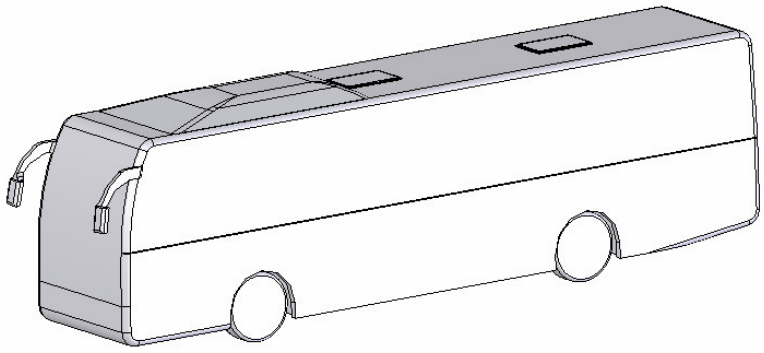

Figure 3.3. 3D model of the bus

The design process of determining the shape of the device was basically a trial and error approach. That is, different types of shapes have been modeled and tested on the device at speeds ranging from 50 to 130 km/h within 10 km/h intervals. In the simulation software, the calculation options, mesh generation and other particular parameters related with the flow analysis are left at their default values. Due to the nature of EFD software, only the desired goal, the ambient conditions and the simple flow definitions like the fluid type are defined. The software automatically reconfigures the required parameters to best fit the problem.

In the beginning of the study, the basic shapes have been applied to the vehicle and tested as described above. These basic shapes simply have the profiles of a half cylinder, a triangle, a rectangle with chamfered edges and an oval shape (Fig.3.4).

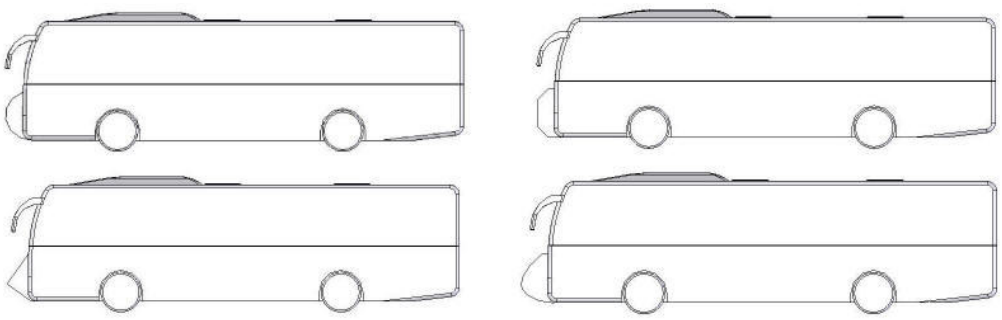

Figure 3.4. Basic shapes attached on the bus

The idea behind testing these different groups of shapes is to find out, at least in a broad sense, their effect on the flow. Therefore, it is preferred to do the analyses in two dimensions (2D). The benefit of 2D analysis is that the calculation time is much shorter to that of 3D analysis. In addition, 2D analyses may provide a reliable estimate on how the different shapes will behave in a full 3D analysis. The goal in the analyses is set as the Force affecting the model in the direction of flow, which in other words is the Drag Force affecting the model. The results of the tests for the initial shapes are listed in Table 3.1 and Figure 3.5.

Table 3.1. 2D Analysis results for the basic shapes

	Experienced Drag Force (N)			
Air Speed(km/h)	Half Cylinder	Triangle	Rectangle	Oval
50	115,405	135,005	112,298	106,848
60	171,781	200,4285	166,2925	158,651
70	228,156	265,852	220,287	210,454
80	303,207	352,7925	292,3175	280,0765
90	378,258	439,733	364,348	349,699
100	472,471	551,229	454,8215	435,236
110	566,683	662,725	545,295	520,773
120	680,405	796,281	654,987	625,125
130	794,127	929,837	764,679	729,477

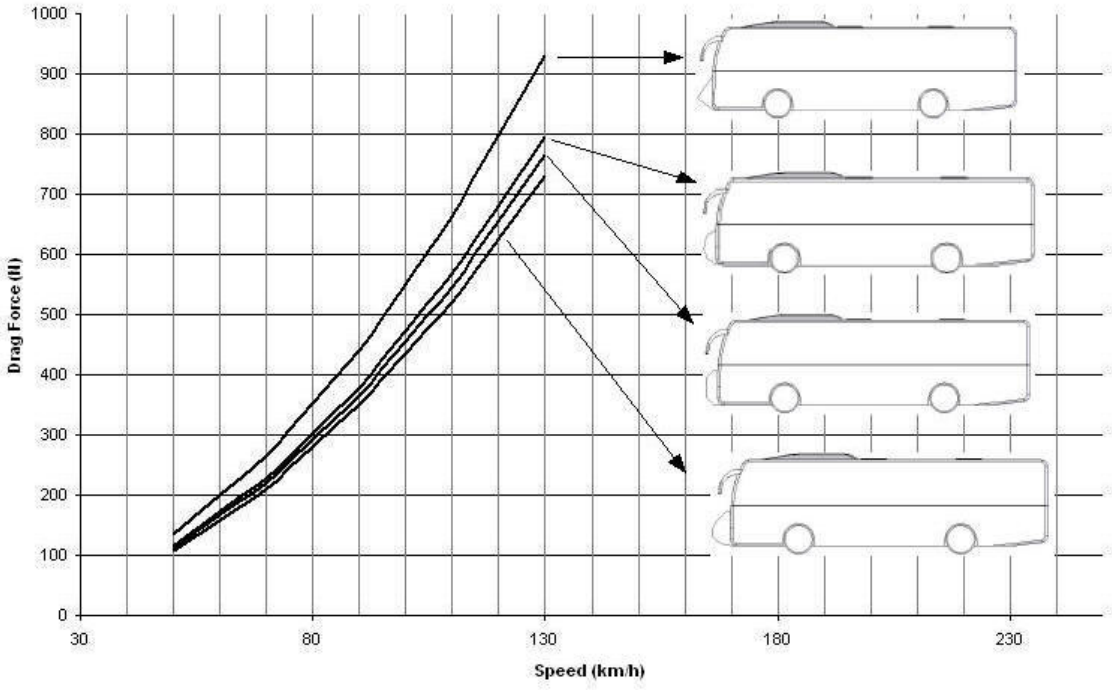

Figure 3.5. Graphical representation of the drag force on the different models

As it can be clearly seen from the tabulated results and from the above graph, each shape experiences different amounts of drag force. The graph also shows how the drag force is increasing with the speed. The obtained results show that the least drag force

was experienced by the oval shaped device. When plotting the reduction in drag forces with the respective air speeds for these shapes it can be seen that as the air speed increases, the efficiency of the devices also increase. This can be seen in Figure 3.6, where at 130 km/h air speed; more than 450 N of force is reduced by the device.

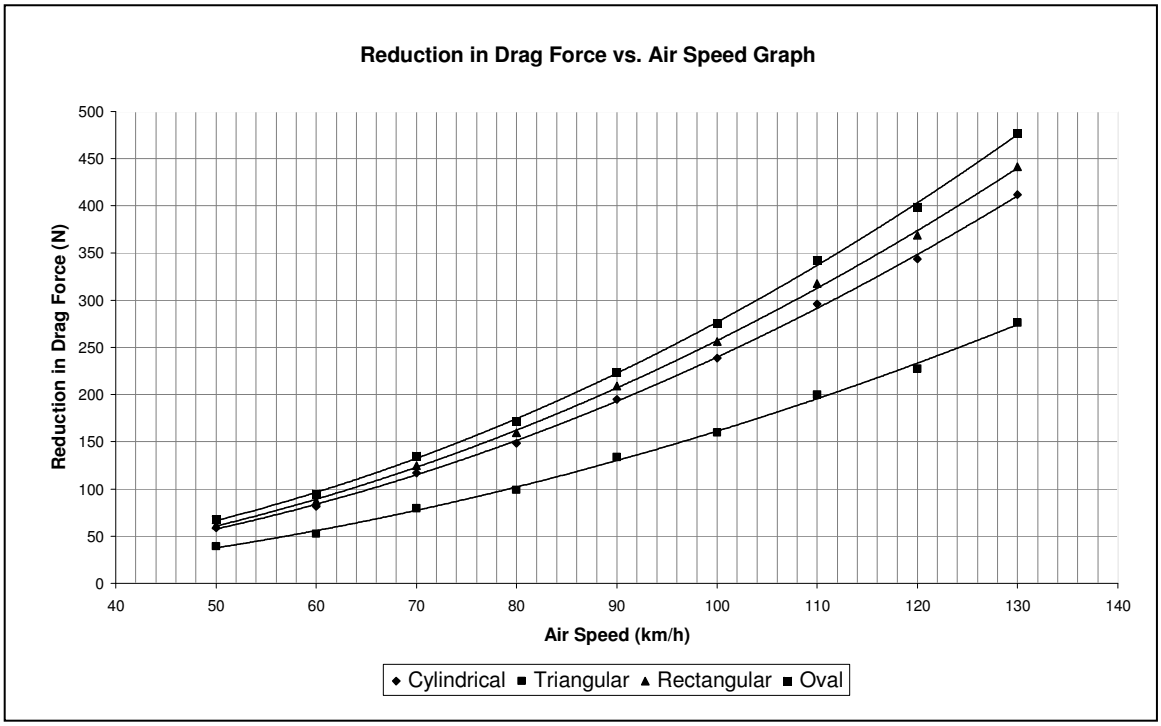

Figure 3.6. Reduction in drag force with the air speed

The effect of the devices over the Coefficient of drag of the bus is visualized in Figure 3.7. It can be seen how each of the devices change the coefficient of drag value of the bus. The plain bus, which means there is no device attached to it, shows the greatest coefficient of drag. The oval shape also produces the smallest coefficient of drag value.

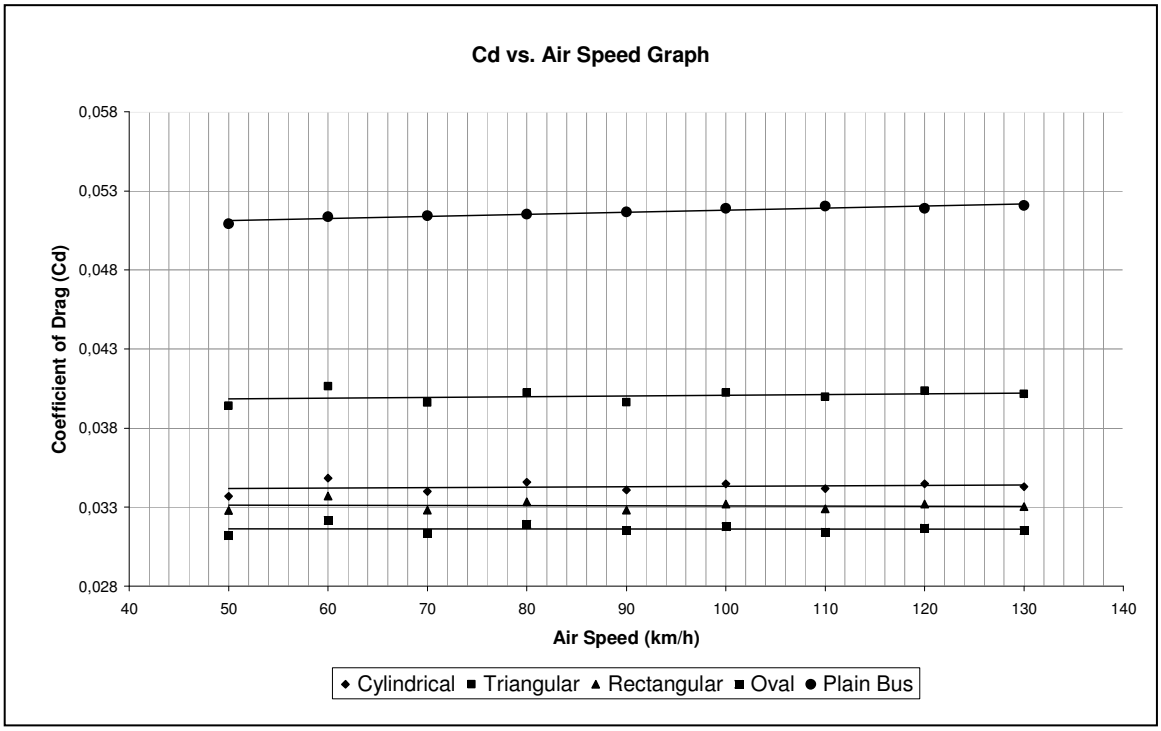

Figure 3.7. Change in Coefficient of drag value with air speed

After observing the results that the oval shape is the most efficient one in terms of reducing the drag force, the research on the shape design was focused on this oval shape. Based on the initial shape, different variations of it have been designed and modeled. These variations are made basically by changing the length or L parameter of the initial shape (Fig.3.8). The other parameters, D and H, are the same for each shape.

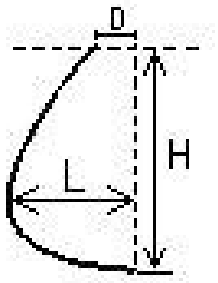

Figure 3.8. Basic curve which is modified with changing the L parameter

By varying the L parameter, thirteen different shapes have been derived (Fig. 3.9).

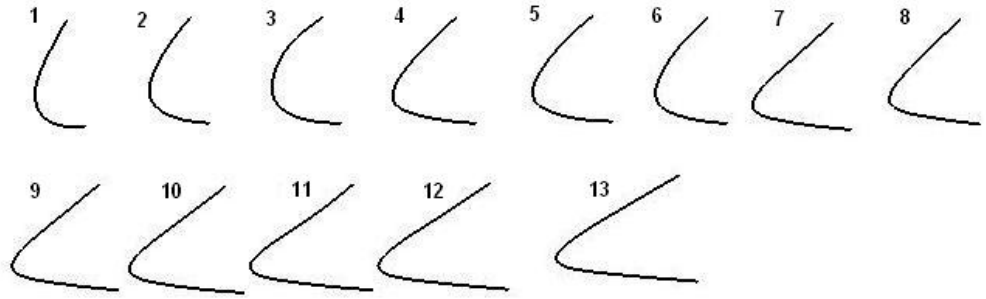

Figure 3.9. Variations of the oval shape

The L parameters for these shapes are given in Table 3.2.

Table 3.2. The L parameters of the shapes

Shape	L (in cm)
1	62
2	70
3	80
4	84
5	96
6	98
7	111
8	117
9	126
10	137
11	147
12	156
13	170

These shapes, which in fact are two dimensional curves, can be defined mathematically with a 10^{th} degree polynomial. When defining the curves in the

Cartesian coordinate system, the lower end of the curve is placed at the origin. According to this, each of these curves can be written in the form as;

$$y(x) = ax^{10} + bx^{9} + cx^{8} + dx^{7} + ex^{6} + fx^{5} + gx^{4} + hx^{3} + ix^{2} + jx + k \quad (3.1)$$

By changing the constants from a through k, all of the above curves can be geometrically defined. In Appendix A the constants a-k for constructing the equation of the curves is given.

Each of those shapes has different geometrical specifications. Rather extreme differences have been also made, to see how they would affect the drag force. Afterwards, each of these shapes has been also tested in a 2D analysis to get an overview on the performances of each shape. The results of the analyses are represented in Table 3.3. In Figure 3.11 it can be seen how the drag force on the bus changes when the devices are placed, and how the fifth device, or shape, experiences the least resistance. In the next plot, it can be seen how much drag force is reduced by the devices at different air speeds (Fig. 3.12). After plotting the Cd values for the devices at each speed level, it can be seen how they are different for each shape and tend to produce a straight line. The R^2 shows that how well the data fit into the straight line function. If R^2 is 1, then the proposed fitting curve coincides with the data.

Results showed that the fifth one experienced the least drag force at each speed level. Therefore after this stage, the process was focused on that particular shape (Fig. 3.10).

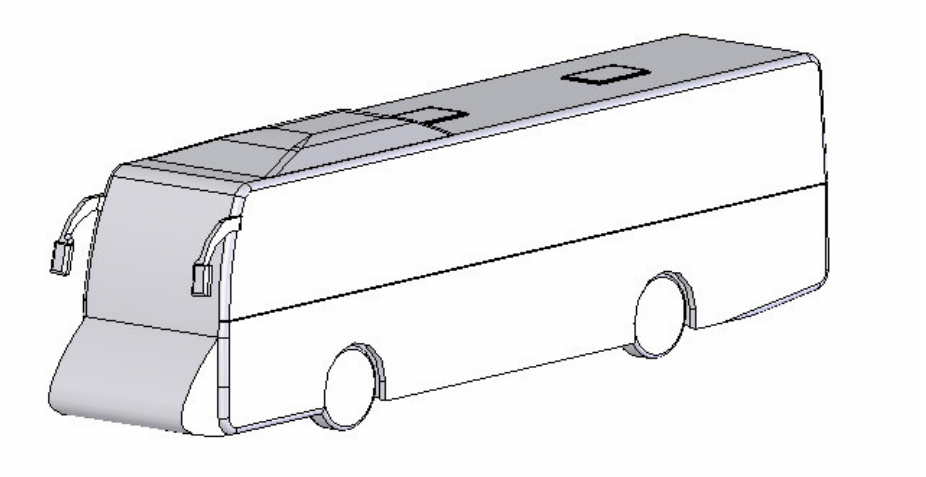

Figure 3.10. The device shape with best performance in 2D tests

Table 3.3. Analysis results

Air Speed (km/h)	Basic Shapes and the Corresponding Drag Forces (N)												
	1	2	3	4	5	6	7	8	9	10	11	12	13
50	159,331	155,369	132,571	132,516	109,105	112,753	138,838	146,112	115,204	128,326	161,192	148,605	116,957
60	230,3	224,913	191,996	191,789	156,962	163,305	200,592	210,649	166,652	185,654	233,048	214,964	167,999
70	320,124	307,932	260,633	262,006	213,788	221,215	274,288	288,588	227,327	251,774	318,325	295,607	230,191
80	410,103	404,472	341,588	343,093	278,332	290,17	358,908	379,122	295,945	330,627	418,258	388,121	300,593
90	531,441	512,786	433,35	436,302	352,886	367,809	456,567	481,832	376,329	419,736	531,144	495,876	380,632
100	659,103	635,472	535,151	539,925	434,942	453,257	563,159	595,894	464,613	519,808	655,954	610,62	472,75
110	802,359	773,06	650,988	654,63	529,221	550,064	682,224	723,277	563,577	631,739	795,769	743,532	571,689
120	957,535	921,246	778,423	783,603	631,416	648,729	812,671	860,676	669,575	747,133	946,94	888,944	679,06
130	1114,58	1083,66	910,448	920,116	740,415	760,301	962,443	1014,58	791,359	879,435	1112,98	1044,23	801,04

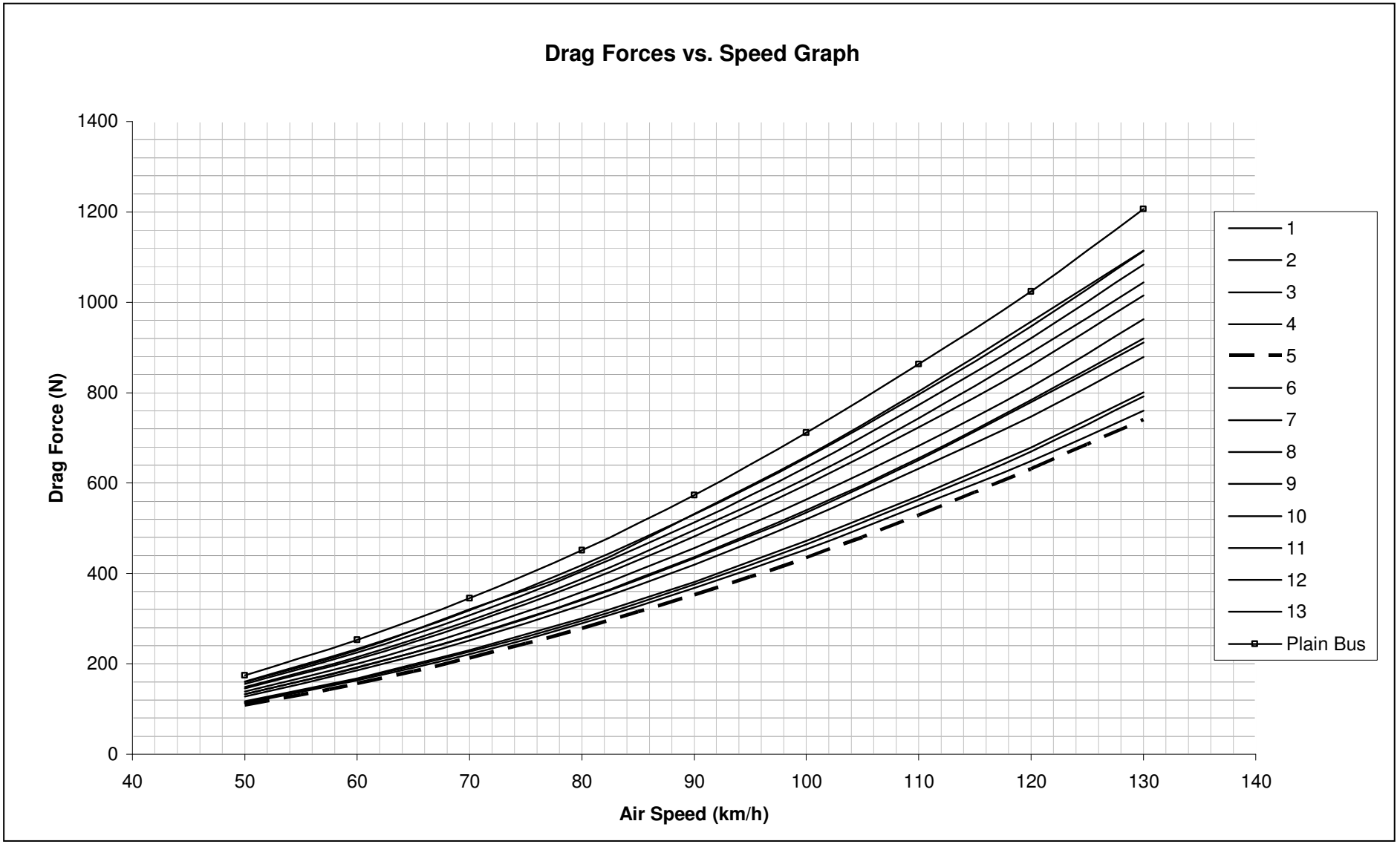

Figure 3.11. Resultant drag force with the different shapes

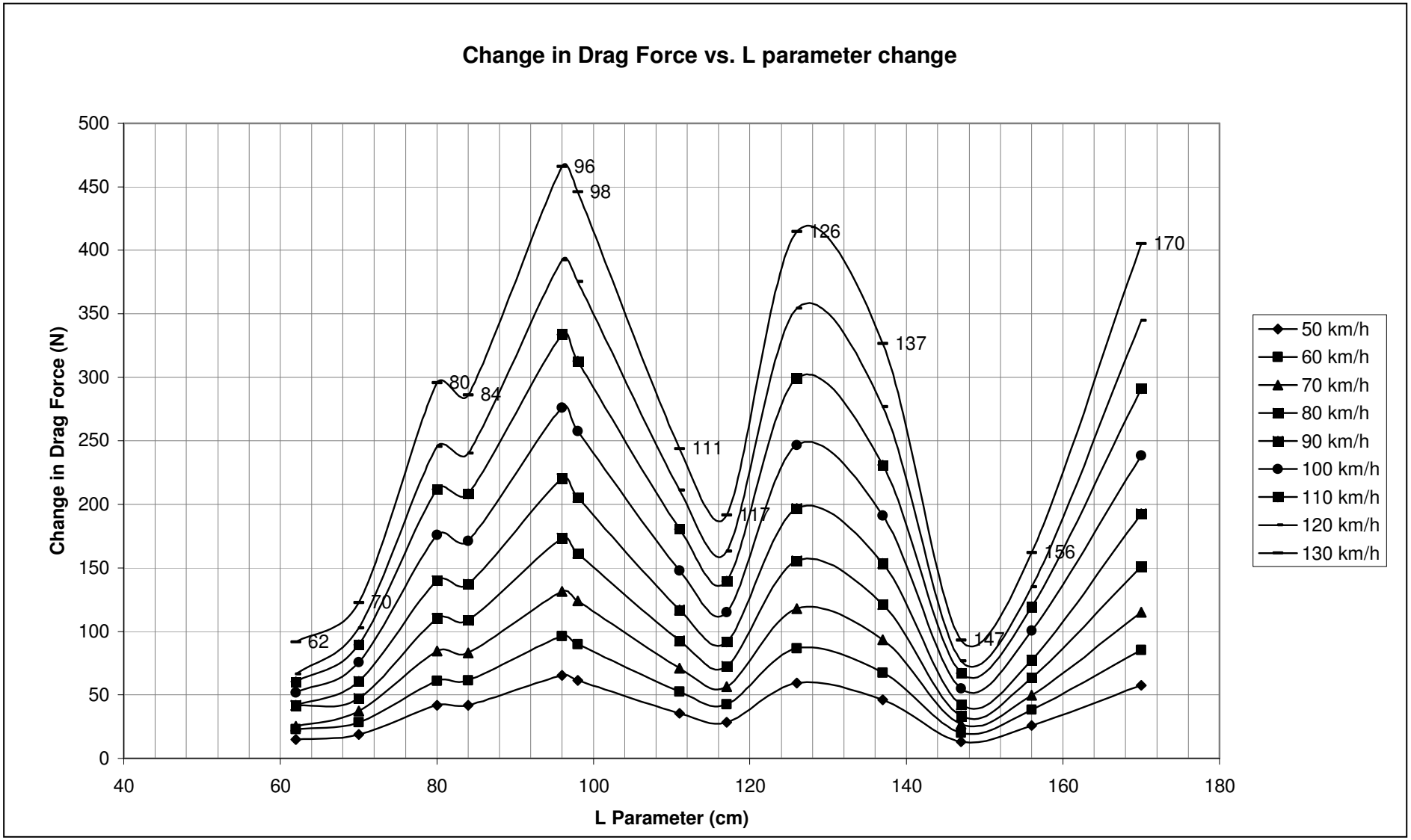

Figure 3.12. Change in drag force with the change in L parameter

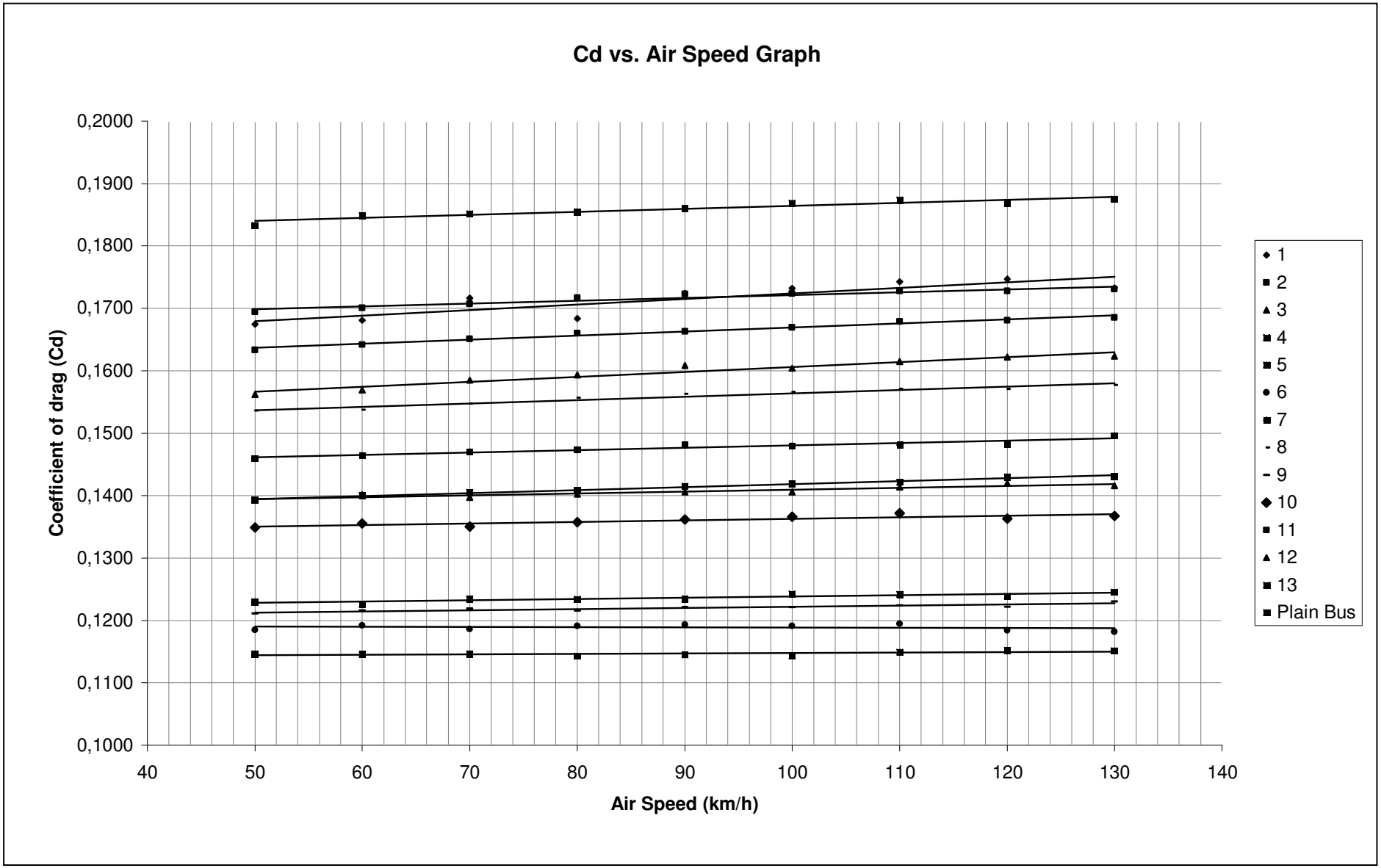

Figure 3.13. Change in the coefficient of drag values with the air speed

By taking the average of the Cd values and tabulating them as below, it can be easily seen that the fifth device produces the smallest resistance to the airflow.

Table 3.4. Equations of the fitting curves for the Cd values of the shapes

	Equation of Fitting Curve	R^2	Coefficient of Drag (Cd)
1	y = 9E-05x + 0,1635	0,7545	0,17
2	y = 6E-05x + 0,1604	0,9752	0,16
3	y = 3E-05x + 0,1379	0,8861	0,14
4	y = 5E-05x + 0,1371	0,9869	0,14
5	y = 7E-06x + 0,114	0,3374	0,11
6	y = -3E-06x + 0,1192	0,0422	0,12
7	y = 4E-05x + 0,1442	0,9143	0,15
8	y = 5E-05x + 0,151	0,9523	0,15
9	y = 2E-05x + 0,1203	0,8054	0,12
10	y = 3E-05x + 0,1337	0,7641	0,13
11	y = 5E-05x + 0,1676	0,9098	0,17
12	y = 8E-05x + 0,1527	0,9449	0,16
13	y = 2E-05x + 0,1217	0,8348	0,12
Plain Bus	y = 5E-05x + 0,1816	0,9024	0,19

In the next steps, the shape designs were merely variations of this shape. In an iterative way, step by step the designs were improved, resulting in a lesser drag force. After a satisfying point was reached in 2D tests, the improved designs were tested in 3D tests. 3D analyses require much more time to complete but it gives a more realistic solution. It was seen from the 2D analysis results that at each speed level, the force reduction rates are proportional. This means, if one shape is more efficient than the other one, then it is more efficient in all speed stages. Therefore in the 3D analysis it was decided that the tests might be conducted at 100 km/h and 130 km/h. The most efficient shape would also achieve better results at the different speeds.

First the plain Bus moving at 100 km/h speed is simulated and a result of 2259.9N drag force is recorded. Then the speed is increased to 130 km/h and a drag

force of 3828.08N is obtained. According to equation (1.1) this corresponds to a Coefficient of Drag value of about 0.59.

The device shapes were accordingly modified in order to meet the three dimensional flow conditions. The right and left ends of the device were cut and rounded so that the airflow may also have smooth passing around the device. The 3D shapes of these devices are also defined mathematically with a polynomial of 10^{th} degree (see eqn. 3.1). For these shapes, a curve profile is used, which in fact is the profile when looking to the device from the side. And to round off the sides another curve profile is used, which simply cuts the shape from the sides. In this way the shapes are represented with two curves. The first one gives the extrusion profile and the second one gives the cut profile for the sides. The equations of these curves are given in Appendix B.

After a series of analysis, a device shape as seen in below figure has resulted in a drag force of 2075.09N at 100 km/h and 3516.96N at 130 km/h, which means a Coefficient of drag value of 0.54. The efficiency in drag reduction of this shape is therefore found to be as 8.5% (Fig. 3.14).

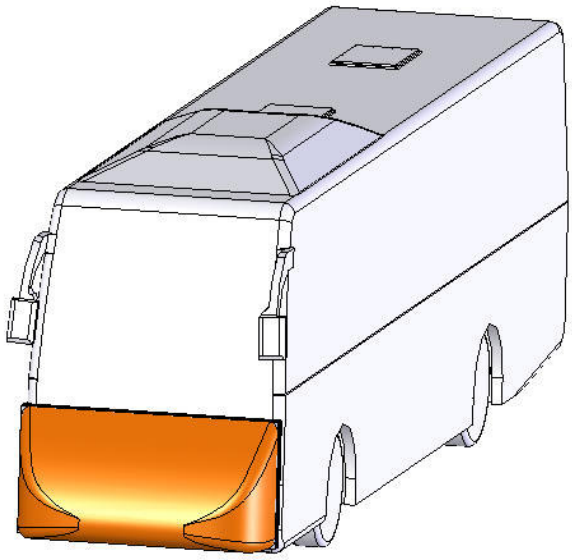

Figure 3.14. Device with a drag reduction rate of 8.5%

In Figure 3.15 it can be seen how the air flow is moving around the bus. It can be seen that the incoming air flow, which hits the front of the bus increases the pressure there.

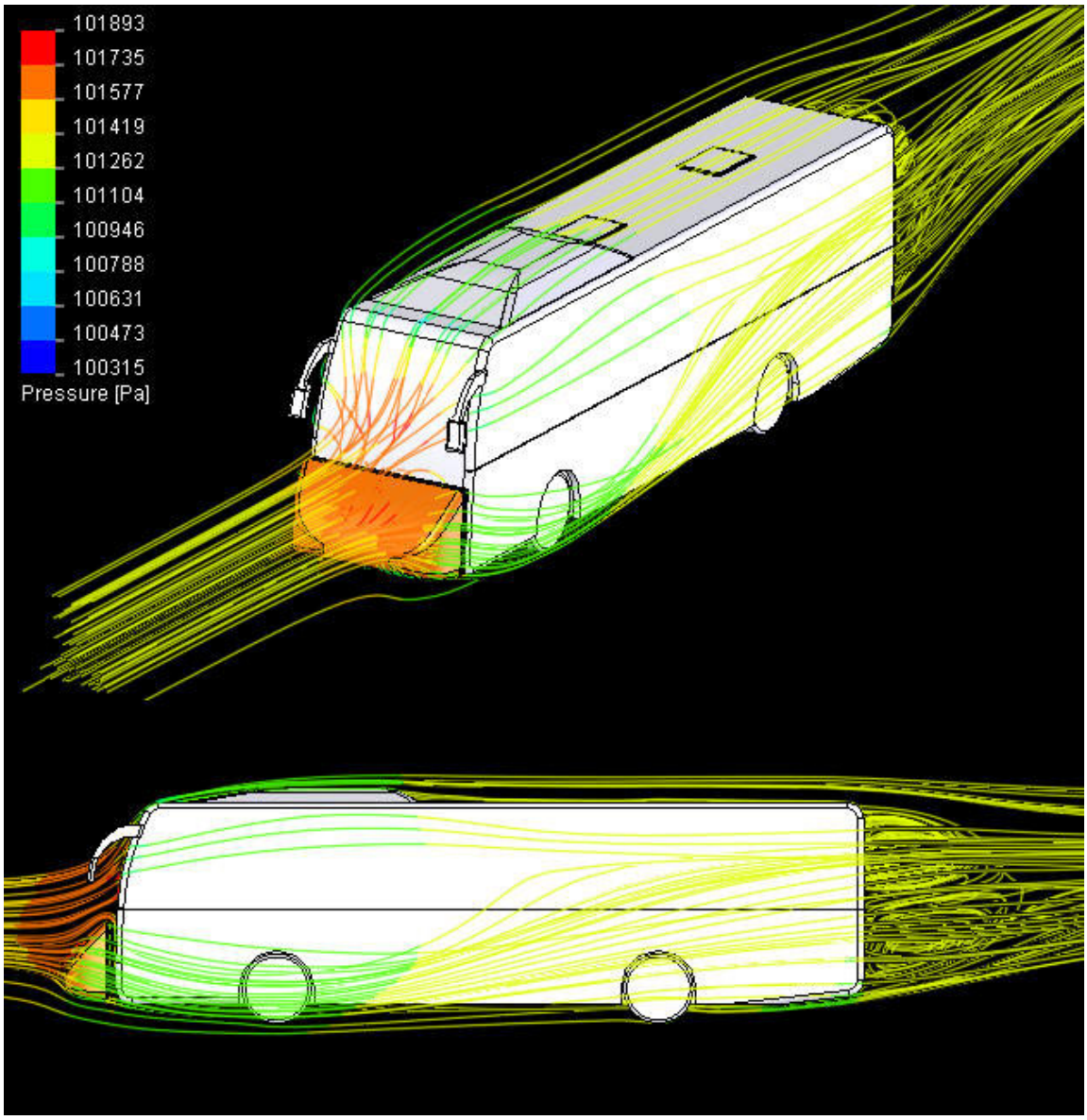

Figure 3.15. Flow lines over the device with 8.5% drag reduction rate

Modifying this design by changing the depth and curvature of the shape, an improved version has been obtained (Fig. 3.16 and Fig. 3.17). This design has reduced the drag force on the bus to 2032.71N at 100 km/h and 3441.96N at 130 km/h, which resulted in a decrease of the Coefficient of drag value to 0.53. With this amount of reduction in drag force, a drag reduction rate of about 10.2% has been achieved.

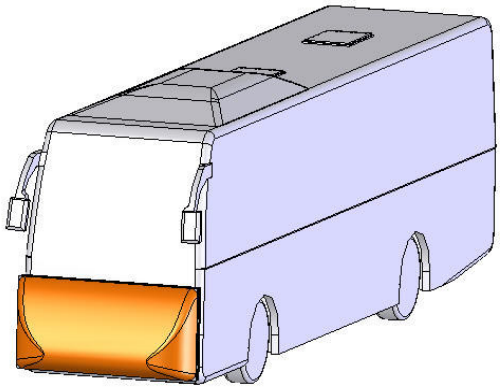

Figure 3.16. Device with a drag reduction rate of 10.2%

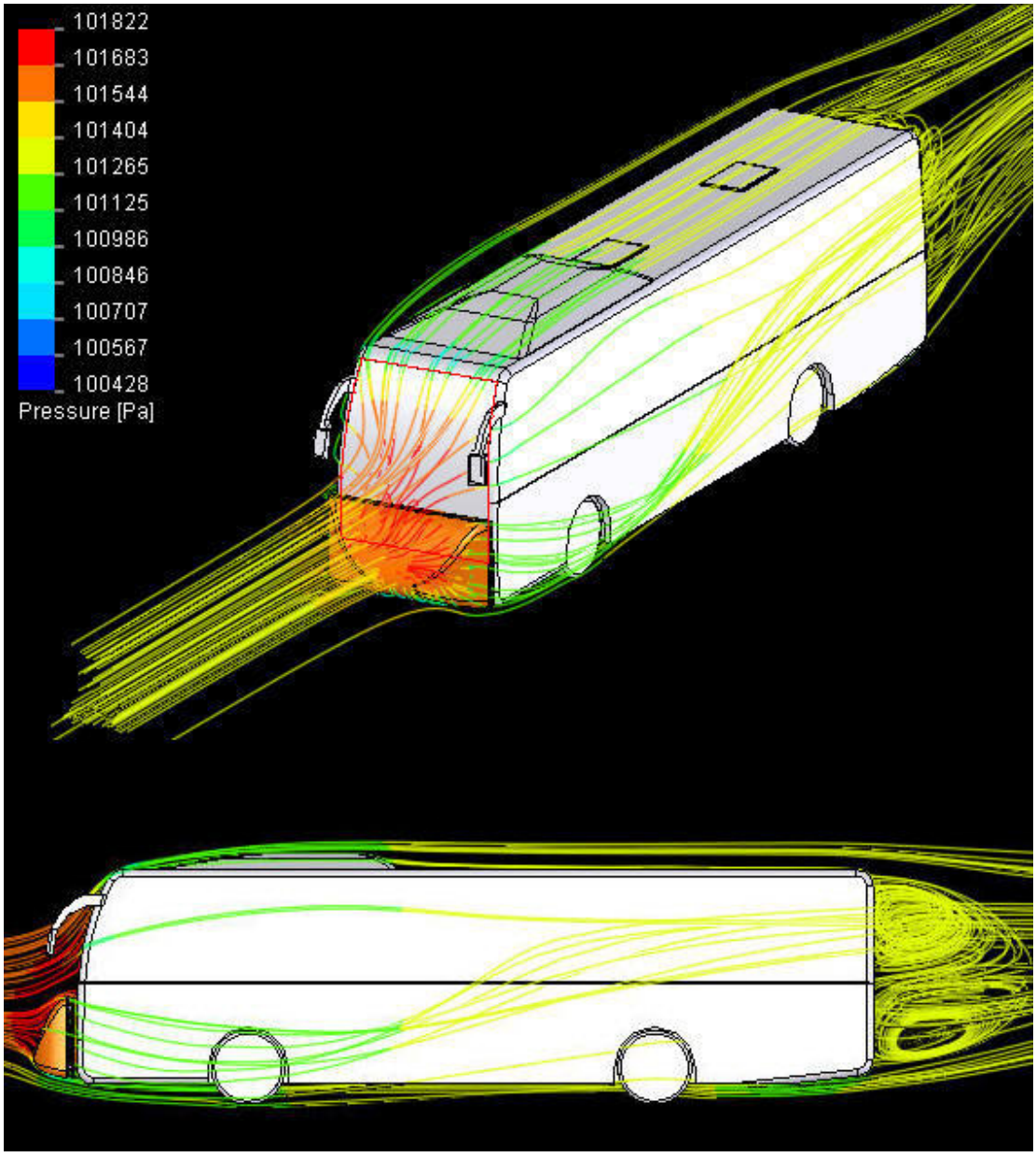

Figure 3.17. Flow lines over the device with 10.2% drag reduction rate

Finally, by changing the geometric properties of the last design an improved design has been obtained (Fig. 3.18). This design has more depth then the previous one but due to its larger curvature radius, the airflow exerts less resistance on it. The sides are curved more and a more smoother flow from the under side to the upper side of the device is made. In Figure 3.19, it can be clearly seen how the pressure increase on the front of the bus is reduced. Hence, in the simulation, the new drag force is found to be 1981.51N at 100km/h and 3348.82N at 130 km/h. This corresponds to a Coefficient of drag value of 0.52. In this way a drag reduction of about 12% has been achieved with this improved device shape. In the ongoing design steps, a better design could not be achieved. Therefore this design is chosen to be the shape of the mechatronic drag reduction device.

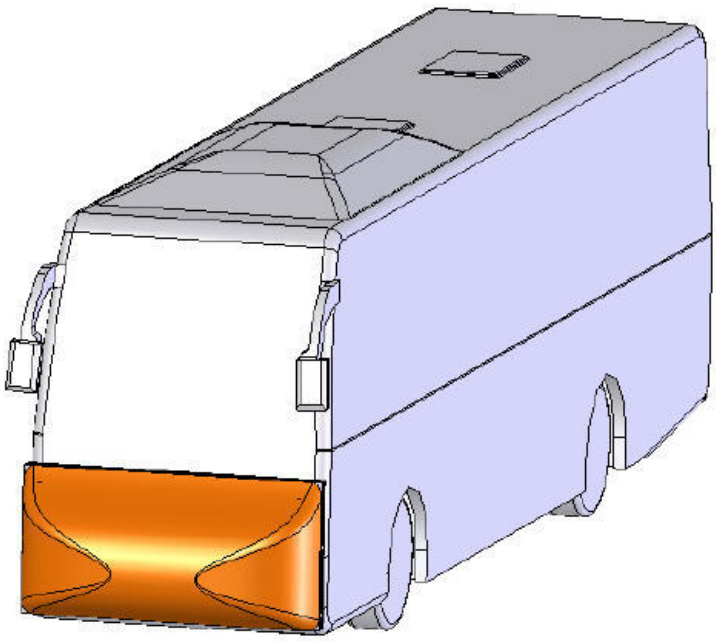

Figure 3.18. Device with a drag reduction rate of 12%

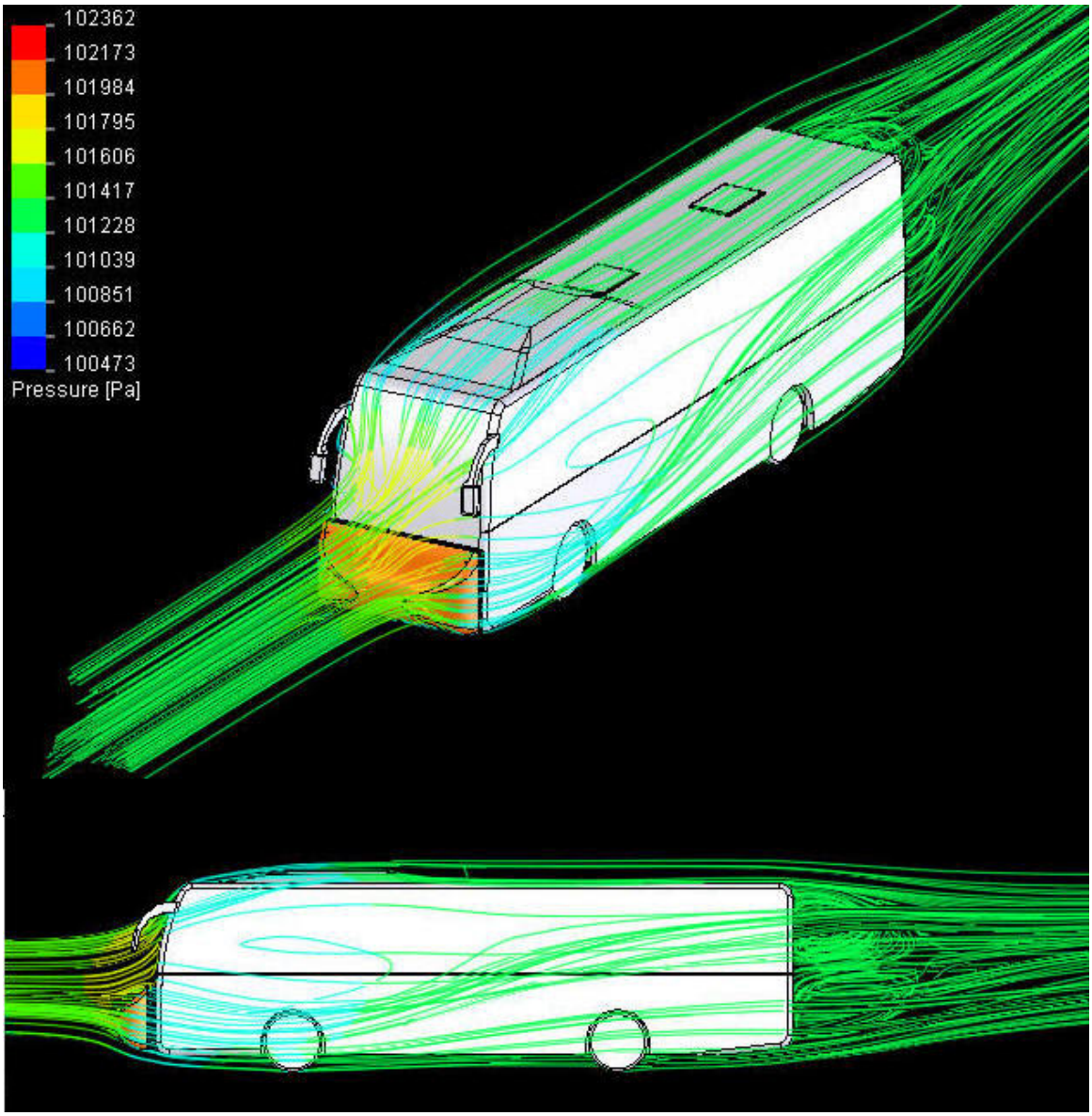

Figure 3.19. Flow lines over the device with 12% drag reduction rate

In the subsequent test and device designs this amount of drag reduction was not exceeded. In addition, this amount of drag reduction rate for an already low-drag experiencing bus is a rather satisfying result. Therefore, this shape was chosen as the device shape that the mechatronic drag reduction device should possess.

3.4. Determination of the Opening and Closing Mechanism of the Device

In the preceding sections it was explained that the device has two states. These are the ON and OFF positions. In the fully opened position the device has to become the shape as depicted in Fig.2.1 and when it is closed it must be able to get smaller and fit into a smaller space. The challenging point in the mechanism design is to achieve a smooth and reliable transition between the opened and closed positions. This section introduces some of the mechanisms that were considered. Both advantages and disadvantages related with these mechanisms are investigated.

3.4.1. Balloon Method

This method is in fact not a mechanism. In this method the device's operation will be very similar to a balloon. That is, the device will be made out of an air proof material, which will be cut and sewed together to that shape. Then this is going to be placed onto the front of the vehicle. To open the device, air is blown into it so that it expands and becomes the predefined shape. The air pressure inside the device must be held at some level, so that the required rigidity of the device is established. Simply, to close the device, the air inside of it is taken out with a vacuum pump and it contracts back. The major advantage of this type of on/off mechanism is that, it is very simple. There are not any motors, linkages or any other system required. The most important parameters which need to be considered are to accurately obtain the desired shape when the device is opening. Another issue is the material selection for the device. It is of primary importance that the material of the device be hard and tough enough, so that during the cruise it will resist outside effects like stones or nails so as not to explode. Also, the required pressure inside the device must be sufficient enough to resist the air pressure outside the vehicle and not deform. Therefore it requires powerful pumps.

The major drawbacks of the balloon method, is the inflation risk of the device. When hit by an object during a drive at high speeds, the sudden impact of the inflating air could probably cause the driver to loose control over the bus. This could unfortunately lead to an accident. Another disadvantage of this type of device could be the risk of deformation of the shape of the device while moving at high speeds or

deformation due to side winds. Since a deformation in the shape of the device directly affects its aerodynamics, any deformation would create an undesirable situation.

Putting all the advantages and disadvantages into consideration, it was decided that this type of opening and closing mechanism would not be a good selection. Therefore another method, the Box method was investigated to be used as the opening and closing mechanism.

3.4.2. Box Method

In this technique the device is divided into four parts. When the parts come together, they form the desired shape of the device by opening like the covers of a box. The device can be divided into four parts; these are the upper right, lower right, upper left and lower left parts. The parts are normally resting on top of each other. When the device starts to open, these parts turn by a desired amount around their turning axes and form the device (Fig. 3.20). The important point in this technique is to achieve a very accurate motion of the parts, so that they flawlessly form the total device. In this method there are two important requirements: angular motion to rotate the parts and a locking mechanism to hold them in position against the drag force.

The Box method unfortunately has some important disadvantages which make it rather inefficient to use as the opening and closing mechanism. One of the most important drawbacks is the space occupied by the device when it is in its closed position. In other words, this type of mechanism does not provide a satisfying amount of volume reduction for the device. Another factor is that this mechanism requires high torque operation since the four distinct parts, which make up the whole device, are to be turned by their turning axis. Also, great precision is required to bring the parts into their correct places and hold them there during the trip.

Therefore, as a third alternative, another mechanism was investigated. This mechanism is called as the Accordion Method and its working principle is similar to that of an accordion.

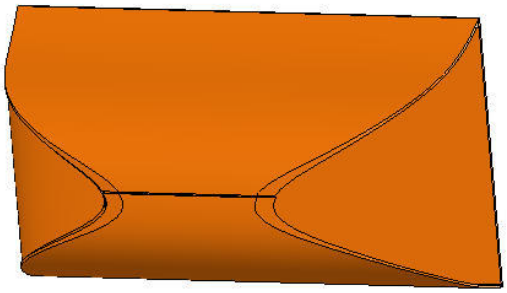

Figure 3.20. 3D representation of the box model

3.4.3. Accordion Method

In this opening and closing technique, the device is composed of five distinct parts, which are simply making up the total device when adding them end to end. When numerating these parts, beginning from the base one attached to the vehicle as number 1, then the most outer one will be number five. These parts are designed so that each part will be able to fit through the previous one. That is number two moves through number one, then number three moves through number two and so on. In this way the whole device is gradually constructed (Fig. 3.21). There will be stoppers in each part, which will stop the next part at some certain distance, so that the original shape of the device can be exactly produced. The closing of the device occurs in a similar way. This time the smallest part, which is the fifth one, starts to move in. Then the fourth part, then the third part and so on, until all parts are retracted back to their original positions. In their original position they sit inside each other and inside the first part. In this way the device's volume is greatly reduced. The advantage of this technique is that it is more stable and reliable than the previous ones. The whole mechanism is driven by a linear motion. However, the drawback is that the device will not have a smooth leveled surface, which means that there will be some level differences between the parts. But this will not cause important problems, since the gaps and level differences between the parts can be sealed or treated with elastic materials in order to fill the gap when the device opens.

After considering these methods of opening and closing, it was decided that the accordion method would be the most suitable in order to achieve the desired motion. In

the next section, the operation principle and a detailed explanation of the opening and closing mechanism is explained.

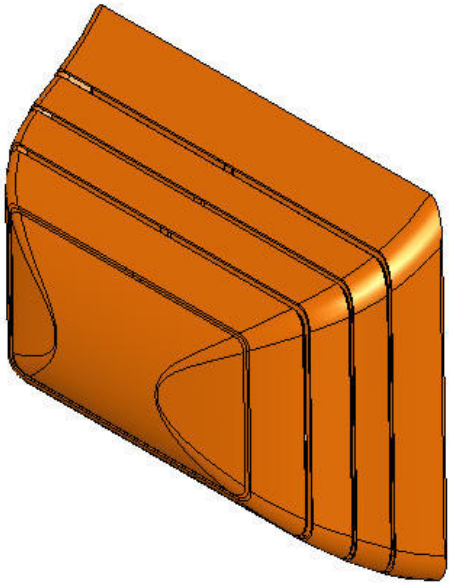

Figure 3.21. 3D representation of the accordion method

3.5. Engineering Calculations of the Mechanism

After deciding the type of opening and closing mechanism, the ways of achieving this task were investigated. As it was broadly explained in the previous section, the device will consist of five parts. These parts will come together and form the desired shape of the device as seen in Figure 2.10. In order to achieve this task, the primary condition is that each part must be able to fit into the previous part. In this way when the device is closed, only the first part, the one attached to the bus, will be seen. When the device opens, the other parts will come out of each other and build the device (Fig. 3.22).

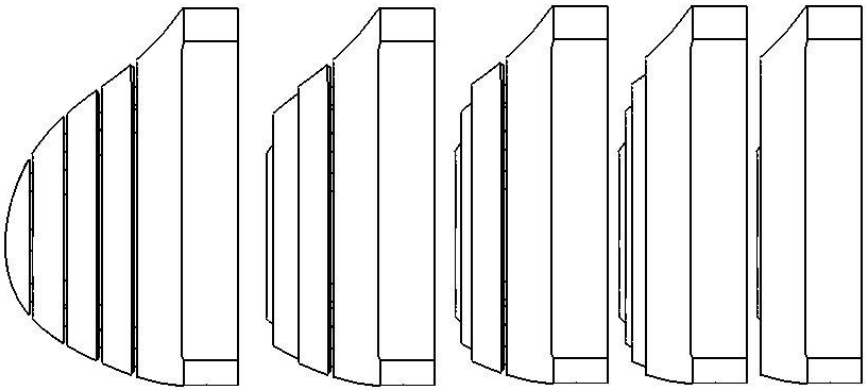

Figure 3.22. States of the device during opening

As it can be seen from the figure above, the mechanism is operated with a horizontal force. In order to provide this horizontal motion, a screw and nut system is going to be used (Fig. 3.23). The green cylinder, which is seen in the below figure represents the motor, is placed on the rotating shaft. The shaft is in fact a threaded shaft, which has opposite threads on the right and left portions of the motor. On the shaft there are two parts which are able to move along the shaft and serve as the connection between the shaft and the links. Since these parts are moving on threads with opposite angles, their motion will also be opposite to each other. In other words, when the shaft turns in a clockwise direction, then the parts will move towards each other and come closer to the motor. However, if the shaft turns in a counter clockwise direction, the parts will expand outward, away from the motor.

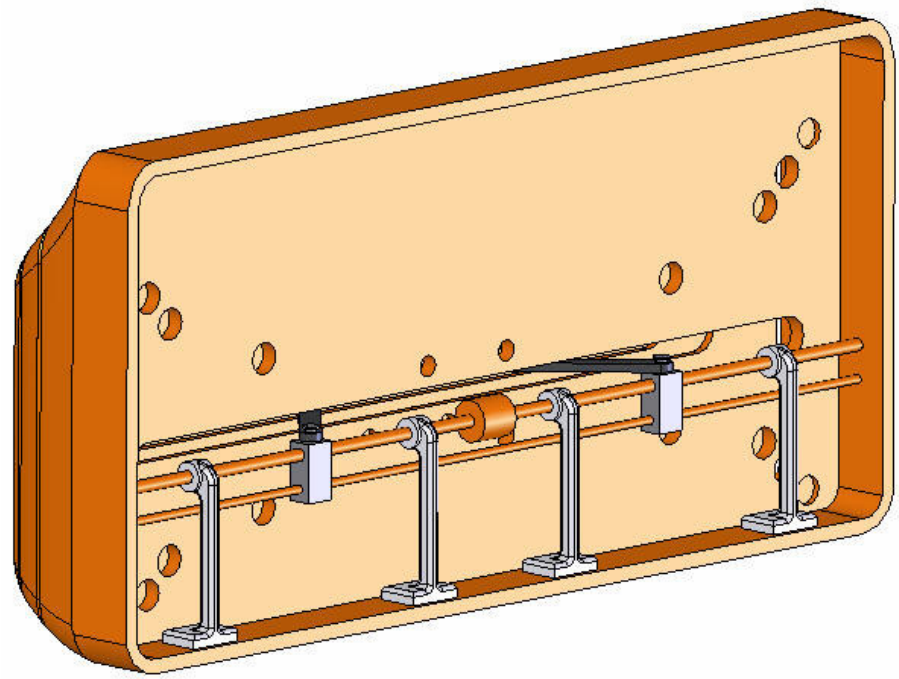

Figure 3.23. Isometric view of the mechanism when open

Under the threaded shaft, there is a smooth finished shaft which basically locks the moving parts, so that they can not rotate. The moving parts have pins on their top surfaces, where the links are connected. The links' other ends are connected to the fifth part of the device (Fig. 3.24).

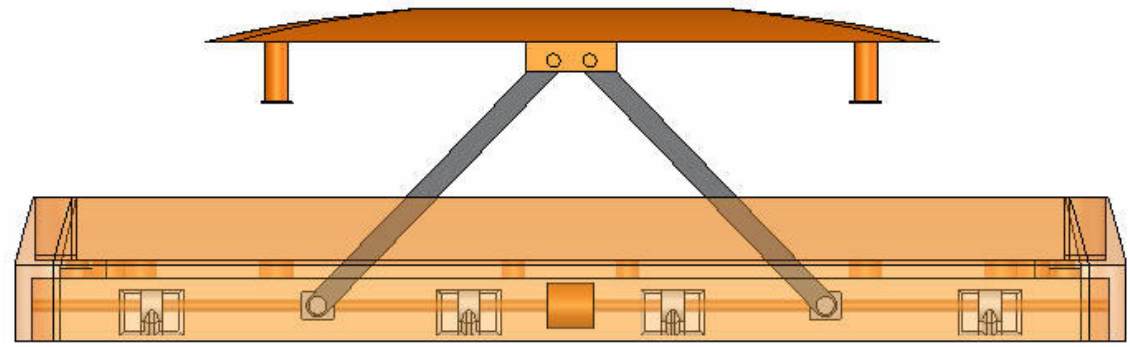

Figure 3.24. The horizontal motion is given to the fifth part

The working principle of this mechanism is very simple. When the shaft rotates in a clockwise direction, then the parts move towards each other. Since the links are connected to the fifth part, they are pushing it forward. Similarly, when the shaft rotates in the opposite direction, the links spread apart and pull the fifth part back.

In order to have this system work, the parts are connected to each other through four shafts placed at their respective corners. In this way the parts can move smoothly inside each other. The cylinders have caps at their ends, so that the parts cannot completely get out from each other (Fig. 3.25). In the opening sequence, first the fifth part starts to slide along the cylinders until it comes to the caps. Then the fifth part moves together with the fourth part. Then fourth part pulls the third part, and finally the system stops when the second part is held by the first part.

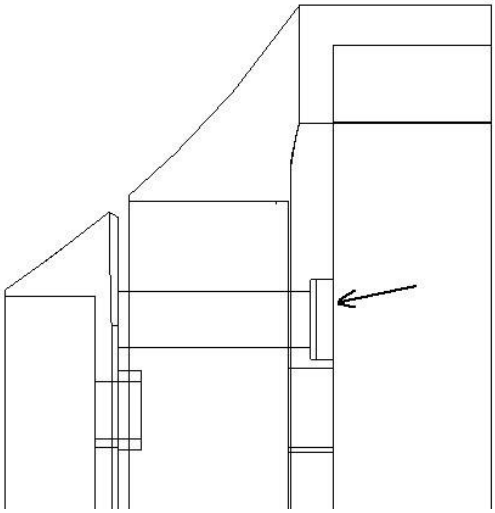

Figure 3.25. The caps holding the parts

Similarly in the closing sequence, the fifth part starts to move back. When it reaches the inside wall of part four, it starts to push it too. When part five and four reach the inside wall of part three, part four pushes part three too. In this way, the parts push each other back, until the second part has reached the inside wall of the first part. In this position the device is closed and all parts rest in the first part. Below in Fig. 3.26, it can be seen how the links move and the system works.

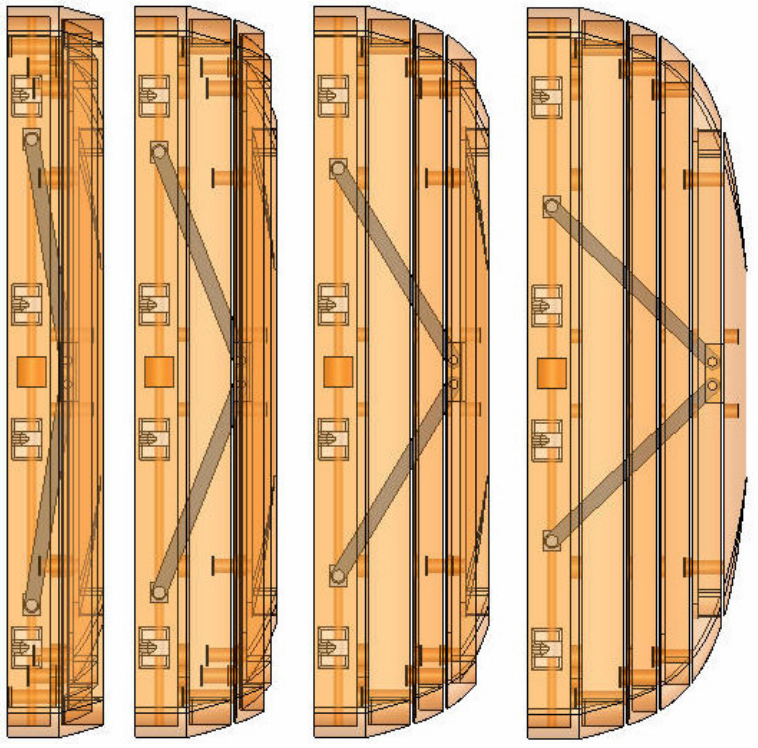

Figure 3.26. View of the mechanism while opening

In the mechatronic drag reduction device it is important that the links, which opens and closes the system, are capable of handling with the forces that occur during their work. In order to prevent any unwanted situations, the links must be chosen of right material. In order to choose the material for the links, a force analysis on the links is made. The analyses are made for one link, since the other link will be the same.

As it can be seen in Figure 3.27, in order to calculate the reaction forces at the points A and C, the drag force has to be determined. The analysis is made for the open position of the mechanism. The Drag Force (Fd) is found out to be around 2000 N, while moving at 160 km/h. Since the system is designed for maximum 130 km/h, a factor of safety of 1.23 is taken applied in the calculations. The links are identical and symmetric about the center, therefore the drag force affecting each link is 1000 N. The lengths of the links are 0.749 m.

As the material for the links and sliders, there were choices available such as steel, iron and aluminum. In this project it was important to select a material with a high strength to weight ratio. This means that a lightweight material with high strength was required. Therefore amongst the other material types, Aluminum 1100 is chosen. The main reason of choosing this type of material is that, it has satisfying strength and is very light when compared to steel. The specific properties of this material are given in Table 3.5.

Table 3.5. Material properties of Aluminum 1100

Aluminum 1100	
Shear Strength	62,1 MPa
Elastic Modulus (E)	68,9 GPa
Shear Modulus	26 GPa
Ultimate Bearing Stress	159 MPa
Tensile Yield Stress	34,5 MPa
Shear Yield Stress	19 MPa

The force analysis according to the first link is shown below.

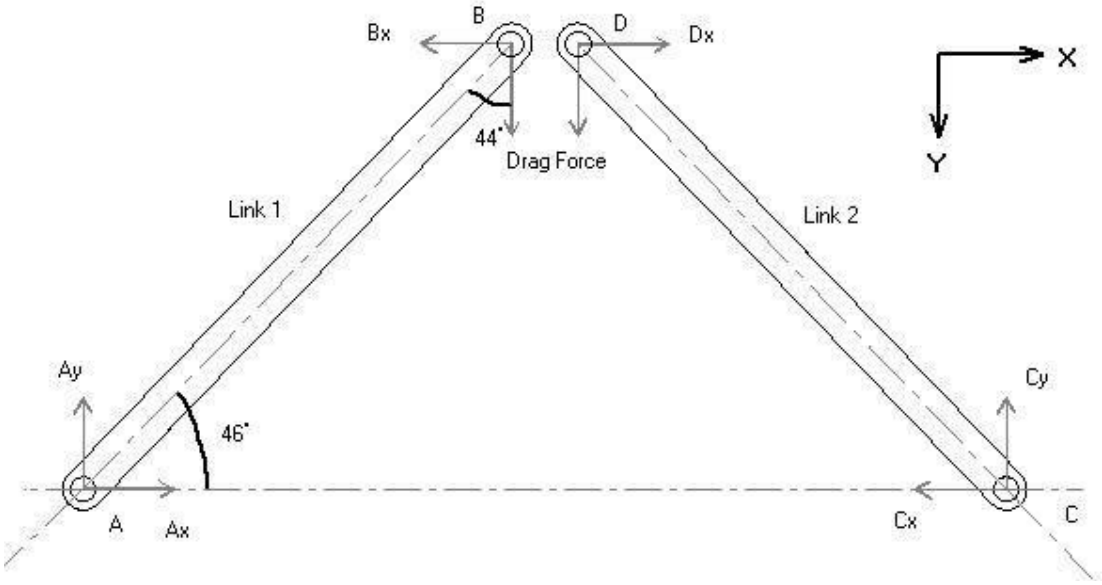

Figure 3.27. Free body diagram of links

Equilibrium of forces along y direction;

$$\Sigma F_y = 0, \quad Ay(-j) + Fd(j) = 0$$

$$Ay = Fd = 1000N$$

Equilibrium of forces along y direction;

$$\Sigma F_x = 0, \quad Ax(i) + Bx(-i) = 0$$

$$Ax = Bx$$

Equilibrium of Moment around point A;

$$\Sigma M_A = 0, \quad (Bx \times l \times \sin 46^\circ)(-k) + (Fd \times l \times \sin 44^\circ)(k) = 0$$

$$Bx = Fd \times \frac{\sin 44^\circ}{\sin 46^\circ} \cong 966N$$

So, the resultant reaction force at points A and C becomes;

$$F_A = F_C \cong 1390N$$

The shear stress occurring at the pins (Fig. 3.28) is found as;

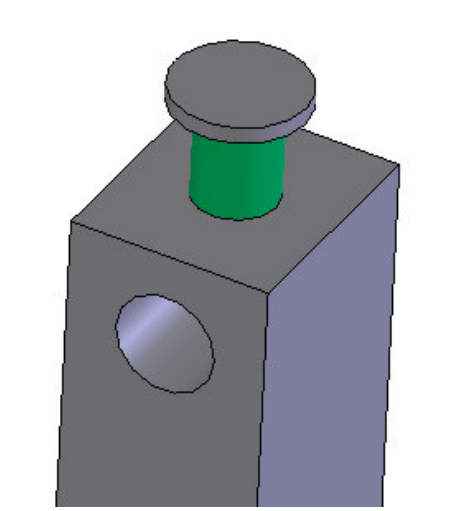

Figure 3.28. Shear stress at the pins

$$ShearStress(\sigma_{Shear}) = \frac{F}{A} = \frac{4 \times 1390N}{\pi D^2}$$

$$\sigma_{Shear} = \frac{6772N}{\pi(30)^2 m^2 \times 10^{-6}} \cong 1{,}97MPa$$

The deflections of the links are calculated (Fig. 3.29);

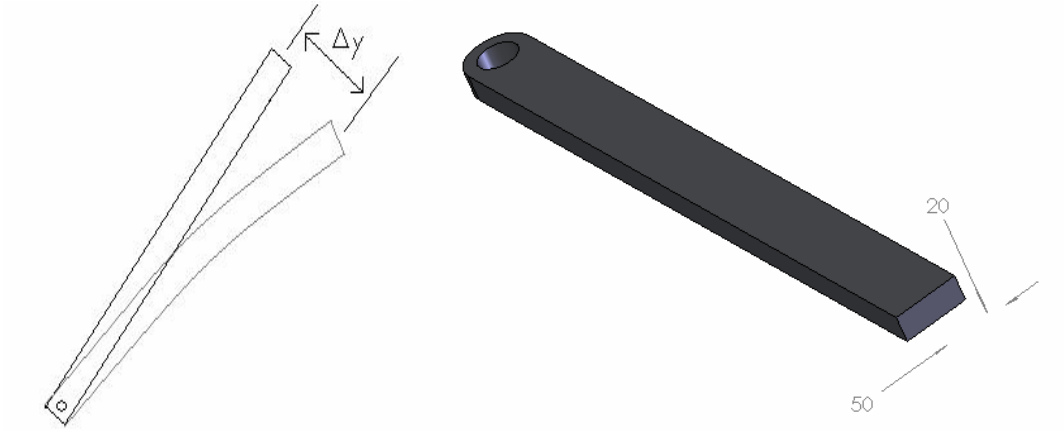

Figure 3.29. Deflection in the links

$$ShearStress(\sigma_{Shear}) = \frac{F}{A} = \frac{966N \times \sin 46° - 1000N \times \sin 44^{\circ}}{(50)(20)m^2 \times 10^{-6}}$$

$$\sigma_{Sheat} \cong 224Pa$$

$$ShearModulus = \frac{ShearStress}{\frac{\Delta y}{L}}$$

$$\Delta y = \frac{ShearStress}{ShearModulus} \times L$$

By replacing the material properties of Aluminum 1100, the deflection becomes;

$$\Delta y = \frac{0{,}97MPa}{26GPa} \times 0{,}749m$$

$$\Delta y \cong 6{,}5 \times 10^{-9}\, m$$

The Bearing Stress in the links;

$$\sigma_{Bearing} = \frac{F}{A_b}$$

Where A_b is the Bearing surface (Fig. 3.30.),

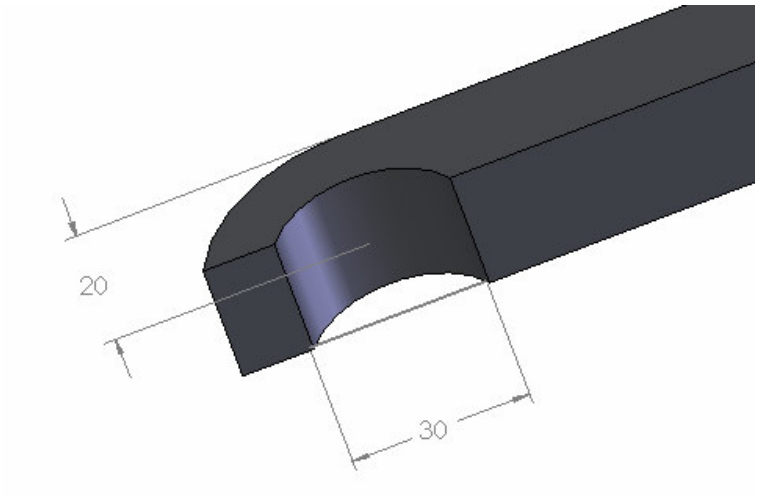

Figure 3.30. Bearing stress in the link

$$\sigma_{Bearing} = \frac{1390N}{(30)(20) \times 10^{-6} m^2} \cong 1{,}61MPa$$

These calculations are made for the critical components; therefore it is assumed that if these results provide an enough factor of safety, the other parts will be safe too.

When comparing the results found above with the material properties in Table 3.3. it can be clearly seen that the chosen material is suitable for the job (Table 3.4).

Table 3.6. Comparison table

Calculated Values	Critical Values	Factor of Safety
1,97 MPa	19 MPa	n= 10
1,61 MPa	159 Mpa	n=99

Another design consideration is the determination of the motor and the threaded shaft. In determining these parts, the most important point is that the torque of the motor will be enough to turn the shaft and resist the axial force along the shaft. Since, the greatest torque will be required during the opening phase; the calculations are made in the open state. Therefore the axial force which the motor must overcome is found, in the previous section as Ax, as 966 N.

The thread is chosen as a square thread, which is mainly used in this kind of applications especially in jacks. The properties of the thread are as follows;

Major diameter, d = 30 mm
Pitch, p, = 4mm, double threaded
Coefficient of friction, $\mu = 0.08$
F = 966 N

The mean diameter, d_m becomes;

$$d_m = d - \frac{p}{2} = 30 - 2 = 28mm$$

The lead becomes;

$$l = 2 \times 4 = 8mm$$

The torque is calculated according to the below equation, which is the formula for jacks torque requirement against the load condition.

$$T = \frac{Fd_m}{2}\left(\frac{l + \pi\mu d_m}{\pi d_m - \mu l}\right)$$

$$T = \frac{966N \times 28mm}{2}\left(\frac{8mm + \pi(0{,}08)(28mm)}{\pi(28mm) - (0{,}08)(8mm)}\right)$$

$$T = 2329Nmm = 2{,}329Nm$$

From this result it can be said that a motor with a torque of 3 Nm, will be enough for opening and closing the device.

3.6. Design of the Electronic Control Unit

The basic operation of the electronic control unit is to provide the communication between the device and the vehicle and to control whether the device works properly. In this project it is not intended to provide a detailed electronic circuit layout for the system. The scope of the electronic design is to identify the operation of the electronic control unit and establish a logical frame for it.

Generally, in most mechatronic systems and devices, the basic task of its electronic system and the control unit is to provide smooth working of the mechanical parts. From this point of view, it can be easily said that, the electronic control unit of this device should be able to control the device parts' opening and closing motions. Therefore the control unit has to control the motor. However, controlling the motor requires a communication and a decision center, which must be able to decide whether to open or not. Since the device is going to be a smart system, it has to control some parameters during the operation. The most important parameter which the device has to keep track of is the outside wind speed, or the vehicle speed. According to these values, the control unit estimates the drag force on the vehicle and decides whether it is necessary to open the device or not. The vehicle's speed can be obtained by using a tachometer and the wind speed can be obtained by air speed measuring devices. If the threshold drag or velocity value for drag or air has been exceeded, then the device decides to open itself. Similarly if the vehicle slows down, then the device automatically closes itself. Alternatively, a direct connection to the driver cabin can also provide a

manual control over the device. In this way the driver acts like a supervisor over the device, and in urgent situations, takes total control over the device.

The electronic control unit also has to take care of the device during opening and closing sequences. Since the opening and closing mechanism is operating in a step by step way, a problem in one step could cause problems in the rest of the operation. Therefore, the control unit has to monitor the mechanism for any problems. Some type of switches placed between the parts could give feedback about the position and condition of the device. In the case of a problem, the control unit should alarm the driver.

3.6.1. The Sensors

Sensors are used to determine the air speed. A sensor is placed onto the front of the vehicle, in order to receive the airflow that would be experienced by the device. The sensor transmits an amount of voltage proportional to the air speed, to the electronic circuit, where it is further processed.

3.6.2 The Circuit

The electronic circuit is the core of the electronic system. It is based on microcontroller technology. The main element is a PIC (Programmable Integrated Circuit) microcontroller. The function of the PIC is to calculate the drag force on the vehicle according to the received values from the sensors. The drag force is calculated according to the general drag force formula as depicted in (1.1). The V values are obtained from the air speed sensors. When the vehicle starts to increase its speed, the air speed sensors will experience faster airflow. Thus, the drag forces calculated by the circuit will become higher. When a certain amount of magnitude in force has been exceeded, the microcontroller will send signals to the drag reduction device and give the ON command. Similarly, if the vehicle starts to slow down and the drag force decreases below a certain limit, the microcontroller will send the OFF command. In this way a simple control algorithm is used to control the drag force acting on the vehicle.

3.6.3. The Motor and Switches

The motor is the actuating device that will bring the mechanism into motion. It is controlled by the signals of the microcontroller and driven through a motor driver circuit. The requirement of the motor is that, it must be strong enough to open the system. In choosing the motor, it is considered that the device should be able to open at higher speeds, where the drag force also has a remarkable effect on the device. Therefore a motor with the required torque calculated in the previous section is required.

The switches are placed inside the device between each stage. The idea is to control whether all stages of the device have been fully opened. The switches also give feedback to the microcontroller so that it knows at which stage the device is and whether it is fully opened or not. If the signals from all the switches are successfully sent to the microcontroller, the microcontroller concludes that the device is opened (or closed) and sends the STOP command to the motor.

CHAPTER 4

DEVICE TESTS

4.1. The Purpose of Testing the Device

Today almost any fluid flow problem can be simulated in computer software. The benefits of these simulation soft wares have been widely discussed in the previous section. It is sure that the simulation results give a good estimate on the flow phenomena and the results. Simulation results may in some cases greatly coincide with the real world results, but in some cases the results can be quite different. Therefore, in most research projects dealing with fluid dynamics, firstly an investigation of the problem and solutions are carried out in computer environment. This greatly speeds up the phase where some solutions and questions about the problem are asked. In other words, computer simulation has a very important effect in understanding the problem and getting answers to the different "If, What" questions. After the solution is greatly evaluated by software simulations, then the validations of these results are made by using wind tunnels or other real condition tests. The main advantage of such a procedure is that, it saves the researcher a considerable amount of time, since doing all of the preliminary tests in wind tunnels would be a huge time, money and effort expense.

The importance of wind tunnel tests can not be neglected. The easiness and wide range of possibilities in simulation software is a major advantage, but since solutions are obtained through ideal conditions and through mathematical expressions they are just estimates for the real conditions. Therefore the same tests are also conducted in wind tunnels to validate the computer simulation results and obtain more realistic solutions. If very carefully conducted wind tunnel tests can achieve an accuracy of about 90%. To perform a useful wind tunnel test, the data obtained from the model should be scalable to obtain forces, moments and other dynamic forces that would exist on the full-scale prototype. There are two basic requirements which must be satisfied in wind tunnel testing.

The most obvious requirement is that the model and the prototype should be *geometrically* similar. That is the relative dimensions in model and prototype should have a constant scale factor.

The other requirement is that the model and prototype flows must be *kinematically* similar. This condition is achieved when the velocities in the flows, in both model and prototype, have the same direction and magnitude which are proportional by a constant scale factor at each corresponding point.

Two flows are *dynamically* similar when both flows have kinematic and geometric similarity. In dynamically similar flows, the identical forces are parallel at each corresponding point and are proportional by a scale factor. In order to achieve the dynamic similarity between the flows, all forces important to the flow must be considered.

The test conditions must be established in such a way that the related forces between the model and the full-scale prototype must be scaled by a constant factor. Only when these conditions between the flows are established, data obtained from the wind tunnel test may be related quantitatively to the prototype flow. To ensure the dynamic similarity between the flows, dimensionless analysis show that the Reynolds numbers in both cases must be the same. In the case of predicting the drag force on a sphere, the results obtained from the model flow can be related to the prototype flow by using the relation of dynamic similarity.

$$\mathrm{Re}_{Model} = \mathrm{Re}_{prototype}$$

$$\left(\frac{\rho VD}{\mu}\right)_{Model} = \left(\frac{\rho VD}{\mu}\right)_{prototype}$$

Thus the drag forces can be related as;

$$\left(\frac{F}{\rho V^2 D^2}\right)_{Model} = \left(\frac{F}{\rho V^2 D^2}\right)_{prototype}$$

As long as the Reynolds numbers are matched, the tests can be conducted in different conditions.

In wind tunnel tests, several factors which greatly affect the results must be considered well. One of them is the detail level of the model geometry. More detailed models which are close to the full scaled prototype may give more accurate results. However, generally this is not the case since all of the details can not be provided in small scaled models. Another important point is the selection of the proper scale for the model. The scale must be chosen according to the wind tunnels test section properties. The wall and ground floor effects are important factors that are affecting the flow of the model. The *Blockage Ratio* must be considered carefully when determining the scale. The blockage ratio is defined as the ratio of the model frontal area to the test section cross sectional area. The blockage ratios can vary according to the conditions, but a value of 5% is sufficient.

The above explained requirements and facts about wind tunnels are thoroughly examined during the research. Apart from the computational simulation, a wind tunnel test was also considered important. In order to provide a test solution for our project, a small scaled Low Speed wind tunnel construction was evaluated. The requirements of the wind tunnel test section depending on the model size are listed in Table 4.1.

Table 4.1. Wind tunnel requirements for different scales

Scale	Air Speed (km/h)	Test Section Cross Section (m^2)
1/50	6000	0,036
1/25	3000	0,146
1/10	1200	0,911
1/5	600	3,643
1	120	91,086

In order to match the Reynolds numbers, as the model gets smaller in size, the required air speed inside the test section increases. Also, depending on the model size, the test section cross sectional area, calculated upon a blockage ratio of 5%, changes. According to results it can be said that as the model gets smaller, a smaller wind tunnel is required. However, in a smaller wind tunnel the required air flow speed, to establish the dynamic similarity, increases dramatically, and vice versa.

Considering the situation and available chances, it was decided that matching the Reynolds number in the wind tunnel would be a very expensive and tedious task. As

it is seen from the table above, in the case of very small models, the amount of air speed which needs to be provided in order to match the Reynolds numbers becomes very high. According to this criterion the maximum air speed required in this project would be 6500 km/h, for 130 km/h simulation. Unfortunately constructing a wind tunnel capable of these speeds is not possible in this project. However, since the important point in doing this wind tunnel tests is to compare the efficiency of different devices on the model, the unmatched Reynolds numbers will not cause a great issue. The differences of the drag forces with each different device attached will show the drag reduction ratio of the devices. However since the Reynolds numbers are not matched, the corresponding drag forces on the original model can not be estimated.

The tests will be done on a 1:50 scaled model bus, which was used as the model in the computer simulations. Since the efficiency of the device and its effect on the air flow, depends on its shape, the wind tunnel tests will be carried out with a passive device. This means that, the device will not be a mechatronic device, but it will be an aluminum block, which is modeled after the determined shape of the device, attached onto the front of the bus. In order to conduct the tests, a simple wind tunnel will be constructed capable of testing the model bus and device.

4.2. Wind Tunnels

Wind tunnel tests are very important in getting information about fluid dynamics. The very early wind tunnels were used in the aviation area, to measure the drag and lift characteristics of different wing types. Since then, wind tunnels have been in use in many different areas, including the automotive industry and other special purposes. Basically, the purpose of a wind tunnel test is to get information on how the tested object reacts to air flow. The objects to be tested can be full scale or model vehicles, building models, ship models or even small city models. Today airplanes and race cars are thoroughly studied with wind tunnel tests. However, it should be also known that wind tunnel tests can not be 100% accurate in simulating real world conditions. In fact, in wind tunnel tests a laminar flow is applied to the object, but in the real world the flow is always in a turbulent form. This makes the wind tunnel test results not identical to the real case. However, in the case of very improved wind tunnels almost 90% of the real conditions can be produced, which means that the obtained

results can greatly represent the real values. Wind tunnels are constructed according to what purpose they will serve. There are very large wind tunnels in industrial use and in important research centers. There are also smaller wind tunnels in universities and schools for educational purposes.

Wind tunnels can be distinguished according to their speeds. For example, wind tunnels testing airplanes and jets are called as Supersonic wind tunnels. These tunnels are able to produce air speeds higher than the speed of sound. On the other hand wind tunnels which produce rather slower air speeds for testing ground vehicles and other objects are called as Low Speed wind tunnels. Wind tunnels can be also divided according to their operation principles. According to this criterion, wind tunnels can be either Closed Loop or Open Loop type wind tunnels.

4.2.1. Closed Loop Wind Tunnels

Closed loop type wind tunnels circulate the air in a closed loop (Fig. 4.1). In this type of tunnel the air is turned at the corners by means of turning vanes. In closed loop tunnels the power loss is less when compared with the open loop tunnels. The major advantage is that the flow can be controlled better, and hence a more laminar and less turbulent flow condition can be achieved. However, these types of tunnels occupy more space and require special attention with the turning vanes and guides inside the tunnel. Leakage is also another important factor which has to be handled carefully. Closed loop wind tunnels are mainly used in big facilities where full scale tests can be performed. Expensive construction costs make these types of tunnels difficult to be used in small scale research activities.

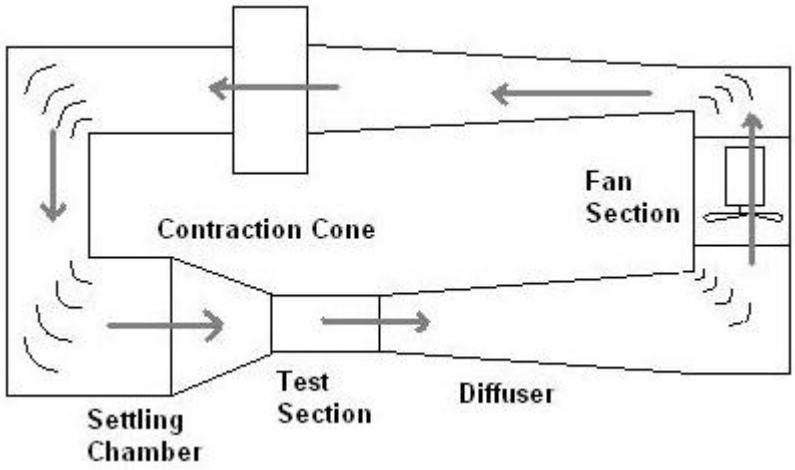

Figure 4.1. Closed loop type wind tunnel

4.2.2. Open Loop Wind Tunnels

Open loop wind tunnels have a rather simple operation principle. The basic difference between open loop and closed loop wind tunnels is that, in open loop tunnels the inlet and exit of the tunnel is connected to the atmosphere (Fig. 4.2). This means that in this type of wind tunnel surrounding air is taken into the tunnel and let out at the exit. This type of wind tunnel is rather uneconomical when compared with the closed loop type tunnel. Another disadvantage is that the flow inside the test section is coming with an outside turbulence; it is not a quality laminar flow. However, this type of tunnel is easy to construct and has very low construction cost when compared to the closed loop tunnel.

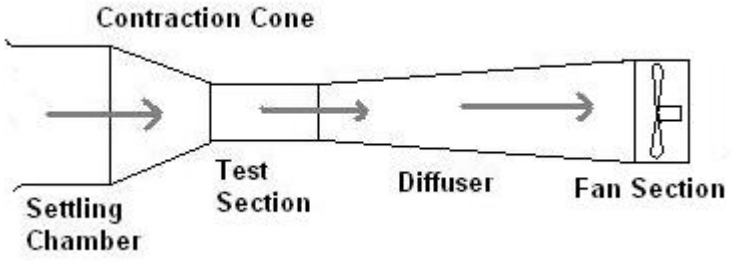

Figure 4.2. Open loop type wind tunnel

After carefully investigating both types of wind tunnels and considering the goals of the project, it was decided that a small scale open loop type wind tunnel would fit into this project. In the next chapter the design of the wind tunnel and its parts will be explained.

CHAPTER 5

DESIGN OF THE WIND TUNNEL

5.1. Parts of the Wind Tunnel

An open loop wind tunnel consists basically of five parts. These parts are called as the settling chamber, contraction cone, test section, diffuser and fan section. The size of the wind tunnel depends on the size of the test section. The size of the test section is determined according to the size of the object to be tested. In other words, the size of the wind tunnel is determined according to the size of the object. In the following sections, the design of the wind tunnel parts is explained.

5.1.1. Test Section

The test section is the section where the test object is placed and the desired measurements are made. The starting point of a wind tunnel design is generally the determination of the test sections size. The sizes are determined according to the size of the object to be tested. When determining the test section size, one must take *Blockage* into consideration. Blockage is defined as the ratio of the largest cross sectional area of the model along the flow direction to the cross sectional area of the tunnel. According to the blockage ratio, the size of the tunnel cross section must be large enough so that the effect of the side walls and the blockage effect of the object do not cause significant errors. Today wind tunnels have different blockage ratios, ranging from 10% to 5%. In this project it is decided that a blockage ratio of 5% is going to be applied. The cross sectional area of the model bus, which is going to be used, is found to be 0.0032 m^2. Therefore in order to achieve the blockage condition, the size of the test section is determined as 30x30 cm (Fig. 5.1). In this case the cross sectional area of the test section will be 0.09 m^2, and 5% of this area corresponds to 0.0045 m^2. As it can be easily seen the area occupied by the model is less than the blockage ratio times the cross sectional area of the tunnel. After the determining the area of the test section, the length of the test section is determined. The important factor in determining the length for the

test section is to have enough length for the flow to combine after it has passed the model. Therefore, for the model bus having a length of 25 cm, the length of the test section is decided as 60 cm. In order to have good visibility during the tests, the tests sections side plates are made out of Plexiglas.

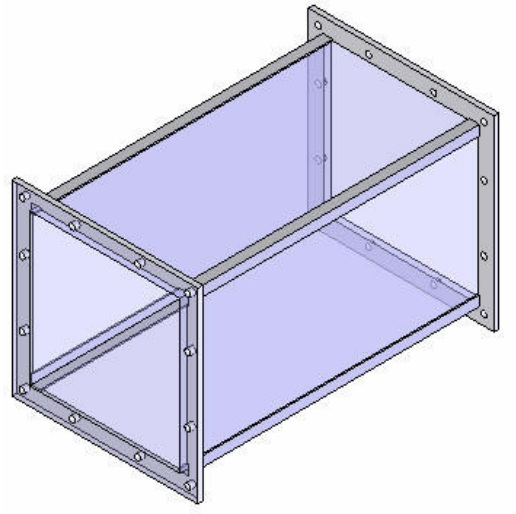

Figure 5.1. The test section

5.1.2. Contraction Cone

The purpose of the contraction cone is to take the low velocity air coming from the settling chamber and accelerate it by passing it through a smaller area to the test section. It is also important that the contraction cone accelerates the high volume, low velocity air with less turbulence. How much the air will be accelerated depends on the contraction ratio. The contraction ratio is the ratio of the inlet and outlet areas of the contraction cone. Keeping the contraction ratio high, will make the air accelerate more, but the occupied space of the contraction cone will become a problem. Different wind tunnel designs have different contraction ratios. In this wind tunnel design, a rather moderate contraction value, a 9:1 ratio is applied. According to this ratio, one end of the contraction cone, the one connected to the test section, is of 30x30 cm. The larger end is of 90x90 cm (Fig. 5.2). The length of the contraction cone is determined as 60 cm. The curvature of the contraction cone is designed such that the air will flow smoothly through it.

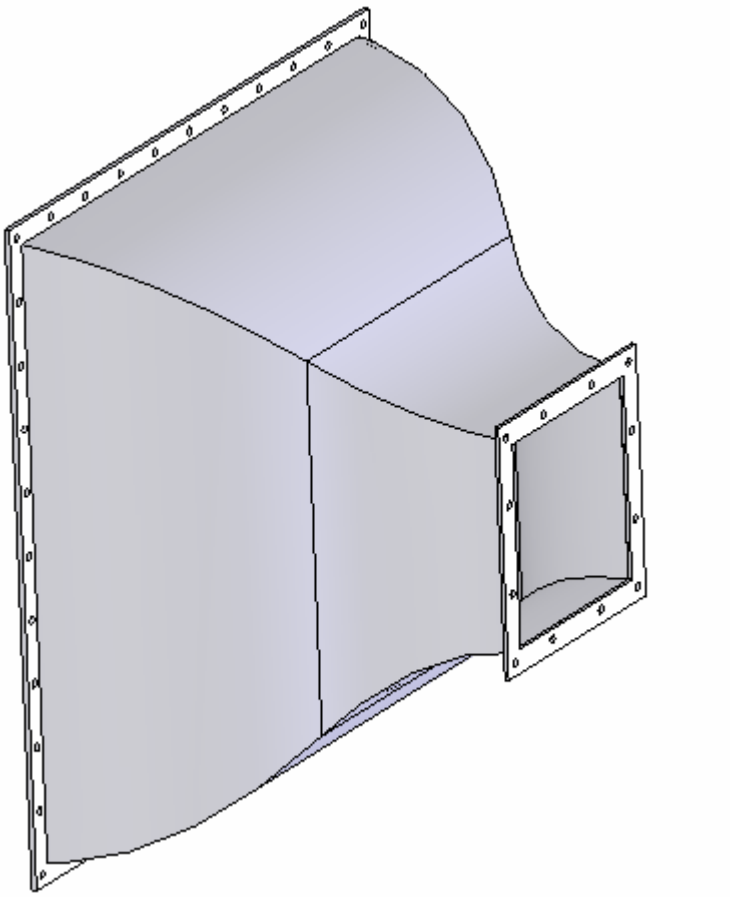

Figure 5.2. The contraction cone

5.1.3. Diffuser

The diffuser lies between the test section and the fan. The primary purpose of the diffuser is to slow down the air speed, as it comes out from the test section. The diffuser also prevents the air stream from turbulating and entering back into the test section. It has a cross section which gradually changes from a square to a circle with an inner diameter of 56 cm (Fig. 5.3). At the end of the diffuser the fan is placed. According to some previous wind tunnel design notes, the departure angle of the diffuser is taken as 4 degrees. The length of the diffuser then becomes 186 cm.

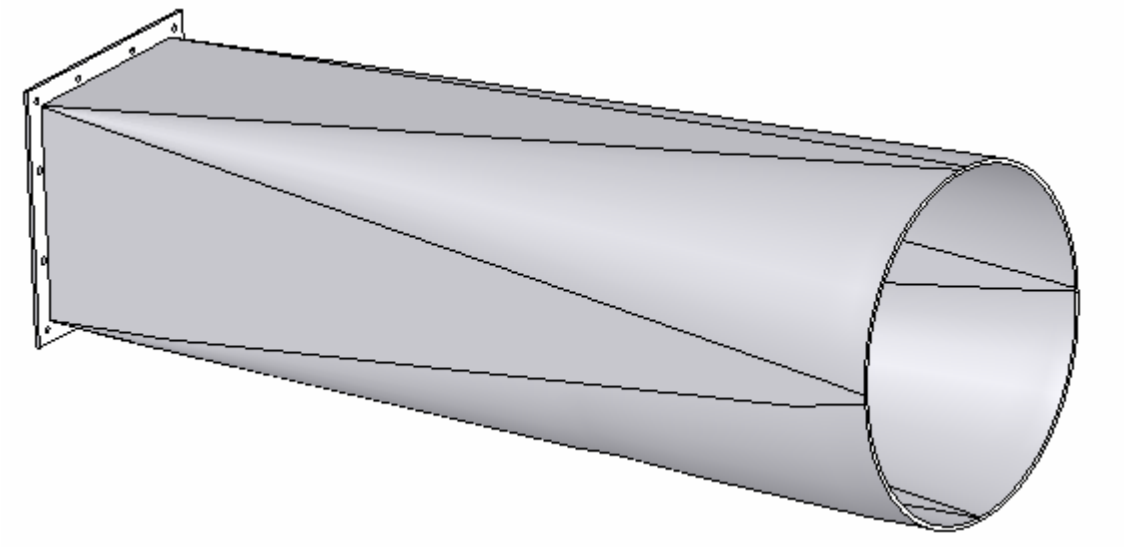

Figure 5.3. The diffuser

5.1.4. Settling Chamber

The settling chamber is placed before the contraction cone, where the air enters the wind tunnel (Fig. 5.4). The purpose of the settling chamber is to straighten the airflow and reduce the turbulence. In order to have a laminar flow condition inside the test section, the settling has some flow conditioning devices in it. These devices basically prevent the swirling inside the airflow and make it flow in one direction along the tunnel. Honeycomb flow straighteners (Fig. 5.5) are placed inside the settling chamber. Other than the Honeycomb structures, two wire mesh screens are also inserted, in order to smooth the airflow.

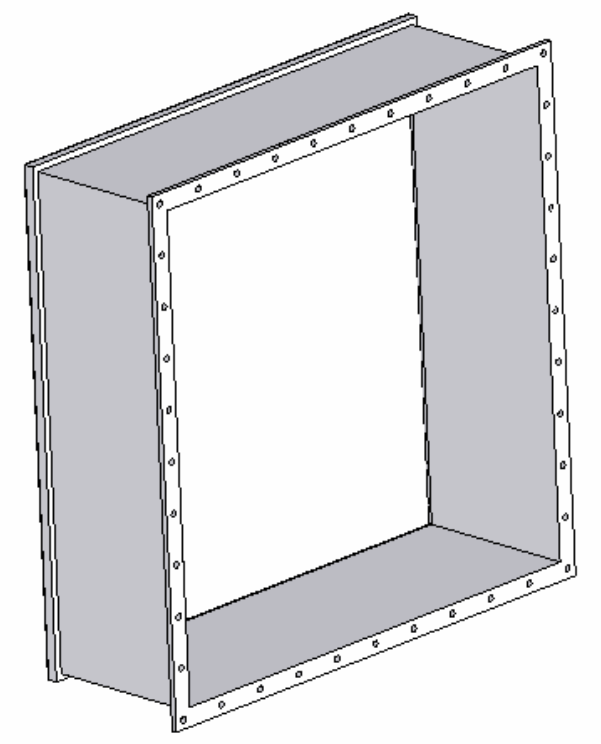

Figure 5.4. The settling chamber

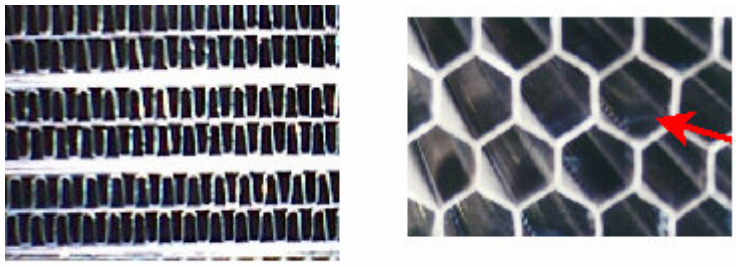

Figure 5.5. Honeycomb flow straighteners

(Source: Web_9, 2006)

5.1.5. Fan

In a wind tunnel the force that drives the air through the tunnel is produced by a fan. It is important that the fan is selected so that it can produce the desired air speed inside the test section and meet the pressure losses inside the tunnel. In this project the

maximum air speed inside the test section is determined as 30 m/s. According to this value, the air flow rate that the fan must have can be easily computed as below.

$$Q\ (m^3/h) = V\ (m/s) \times A\ (m^2) \times (3600 s/h) \quad (5.1)$$

Where Q, represents the air mass flow rate, V the air speed and A the cross sectional area of the test section. If we put the V and A values into equation (4.1), then the air mass flow rate is found as 9720 m^3/h. Also, taking into account the pressure losses in the system, it was decided that a fan capable of producing at least 10 000 m^3/h air flow, could be used as the driving unit for the tunnel.

5.2. Manufacturing of the Wind Tunnel

The manufacturing of the parts explained in the preceding sections, were done by a local enterprise. The wind tunnel parts were made out of sheet metal, by forming processes. The parts of the wind tunnel are separately manufactured and dyed. By bolting the parts together the wind tunnel will look like in below figure (Fig. 5.6).

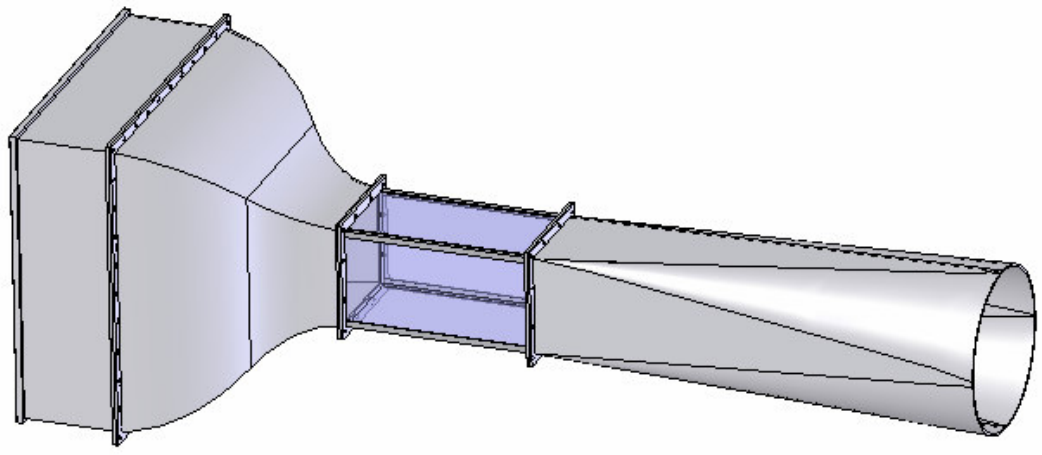

Figure 5.6. 3D view of the wind tunnel

The Fan used in the wind tunnel is a suction type centrifugal fan. It is operated by a 2.2 kW, 1400 rpm and three phase alternative current motor (Fig. 5.7).

Figure 5.7. The Fan

In order to be able to control the air speed inside the tunnel a frequency controller for the fan is required. The frequency controller basically enables the user to decrease or increase the drive speed of the fan. Therefore, a 2.2 kW fan frequency controller from Siemens has been obtained (Fig. 5.8).

Figure 5.8. The frequency controller of the fan

The honeycomb flow straighteners are made out of metal stripes in rectangular shapes (Fig. 5.9)

Figure 5.9. Flow straighteners inside the settling chamber

After connecting the test section to the diffuser and contraction cone, and the fan to the diffuser, the wind tunnel looks like below (Fig. 5.10)

Figure 5.10. The wind tunnel

CHAPTER 6

WIND TUNNEL TESTS

The wind tunnel tests are made with 3 different device shapes. These shapes are the ones which were obtained through the design stage (Fig. 6.1). The devices to be used in the tunnel tests are manufactured from Aluminum (Fig. 6.2) and attached to the model bus and the corresponding drag forces are measured.

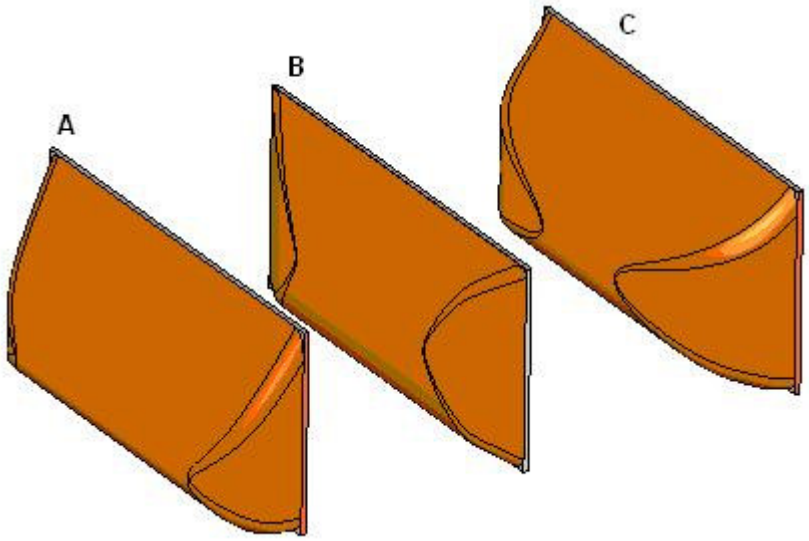

Figure 6.1. The 3d models of the devices tested in the wind tunnel

Figure 6.2. The aluminum devices tested in the wind tunnel

The resulting drag forces are measured with a force measuring system (Fig. 6.3). The force measuring system consists of a lab scale and a weight. Inside the test section, the bus is connected to a string. The string goes around a pulley and its other end is attached to a weight. When there is no air flowing inside the tunnel, the scale will read the weight of the mass hanging on the string. However, as soon as the air speed increases in the tunnel, the drag force will push the bus backwards and cause the weight to lift, thus changing the scales measurement. In this way it will be possible to see how much drag force is affecting the bus at different speeds and with different devices attached. In this way a comparison between the different test speeds and device shapes will be possible.

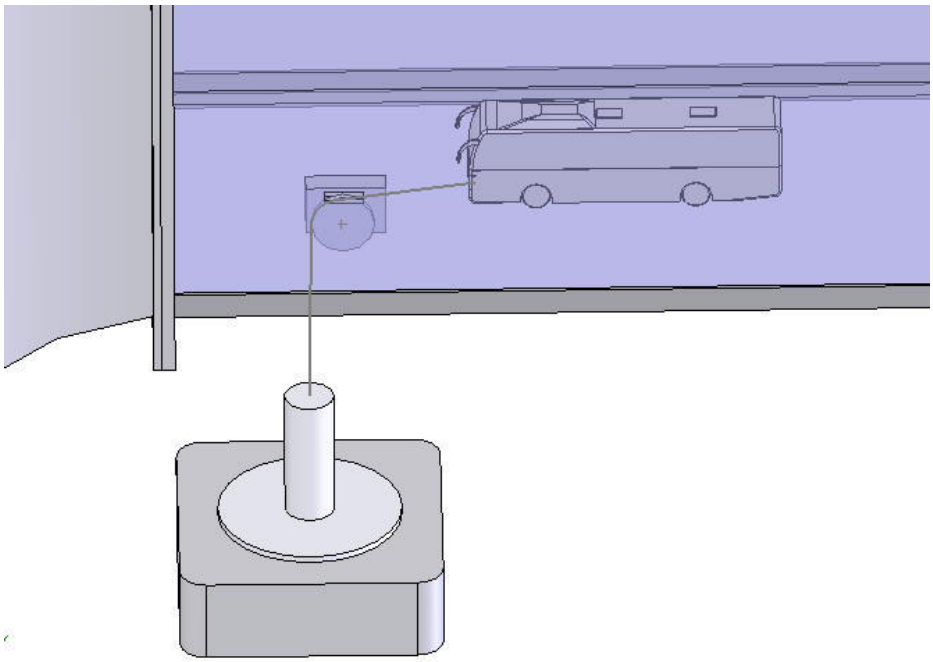

Figure 6.3. 3D view of the force measurement system

In the wind tunnel, the system is constructed by using a pulley made in the machine shop and a scale with ±1 gram tolerance (Fig. 6.4).

Figure 6.4. Force Measurement System

CHAPTER 7

TEST RESULTS

The wind tunnel tests were conducted at different air speeds ranging from 55 km/h to 115 km/h, in 5 km/h intervals. The drag force occurring on the bus is measured in the case of the plain bus, and with the three devices attached. Before conducting the experiments it was estimated that the results would coincide with the simulation results. The wind tunnel tests were conducted six times for each device type and then the average results are used to compare the devices. The obtained average results for the different devices are given in below table. The forces are read as grams from the scale and converted to Newton using the equality of 1kg ≈ 10N.

Table 7.1. Wind tunnel test results

	Drag Forces (N)			
Air Speed (km/h)	Device A	Device B	Device C	Plain Bus
55	0,13	0,12	0,09	0,09
60	0,18	0,16	0,12	0,14
65	0,23	0,20	0,16	0,19
70	0,27	0,26	0,21	0,24
75	0,32	0,31	0,26	0,30
80	0,37	0,36	0,32	0,36
85	0,43	0,42	0,37	0,43
90	0,50	0,48	0,44	0,50
95	0,57	0,54	0,52	0,58
100	0,64	0,62	0,59	0,66
105	0,70	0,69	0,66	0,73
110	0,76	0,74	0,72	0,79
115	0,82	0,79	0,78	0,86

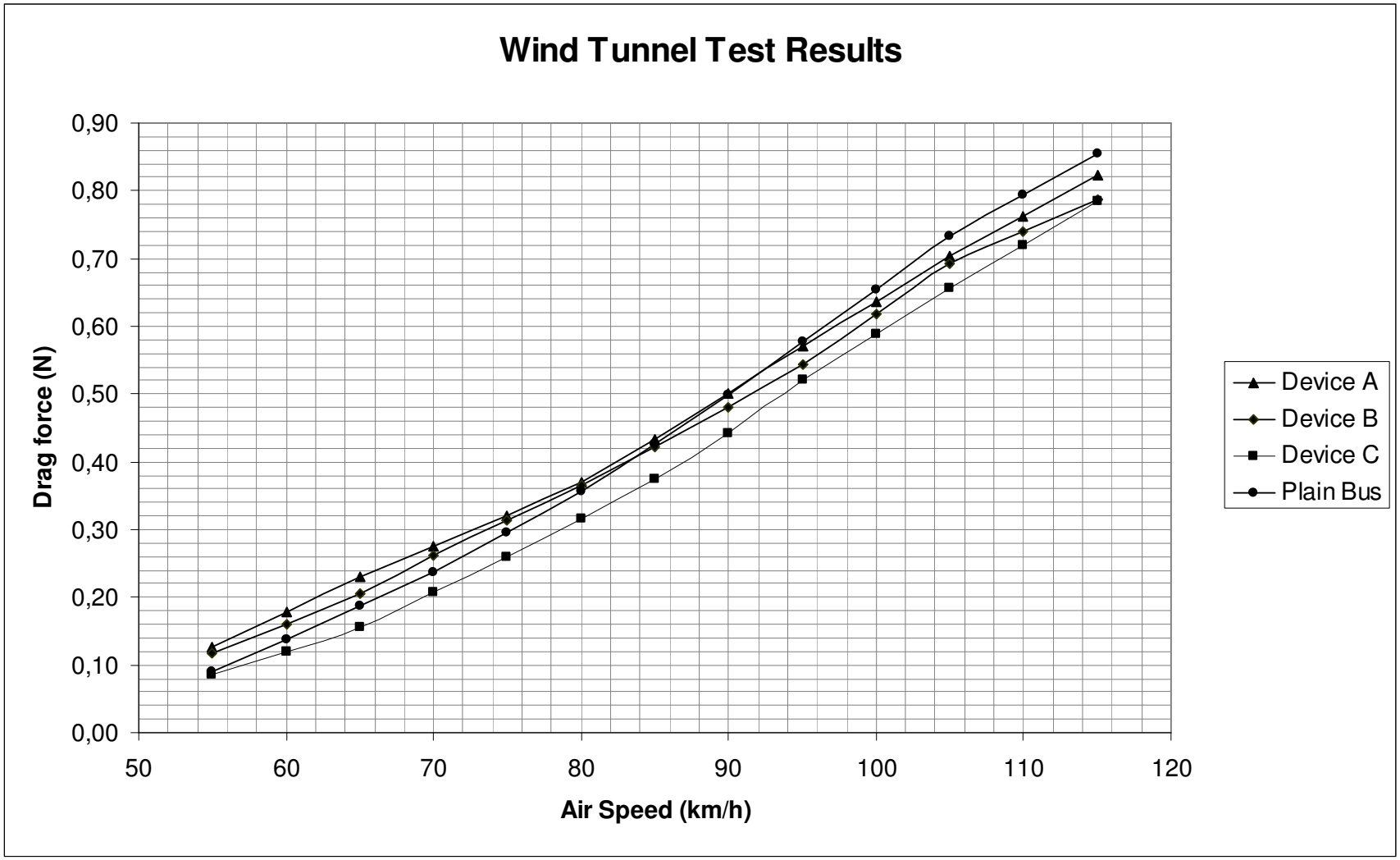

Figure 7.1. Wind tunnel results for the tested devices

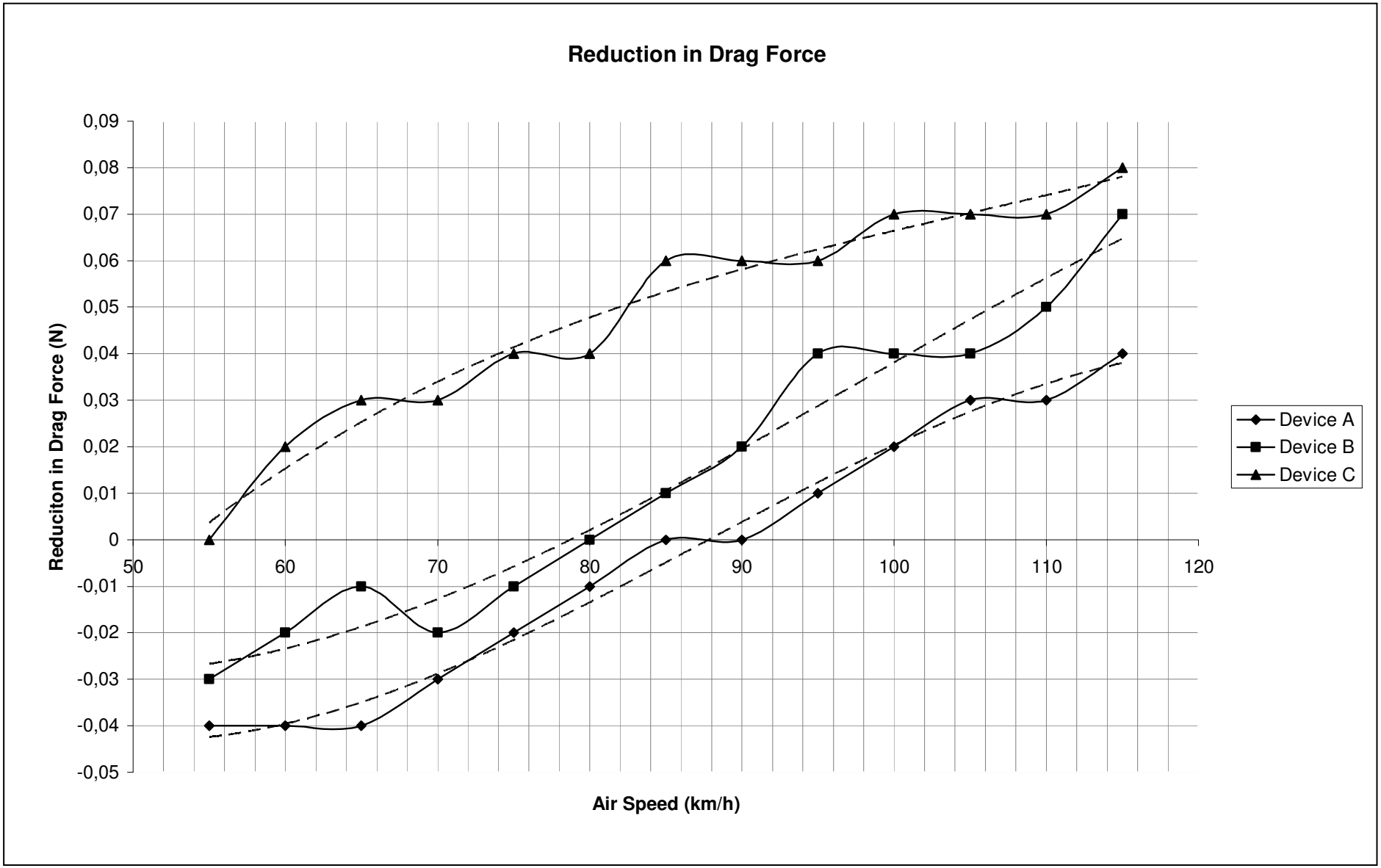

Figure 7.2. Amount of reduced drag force with the air speed

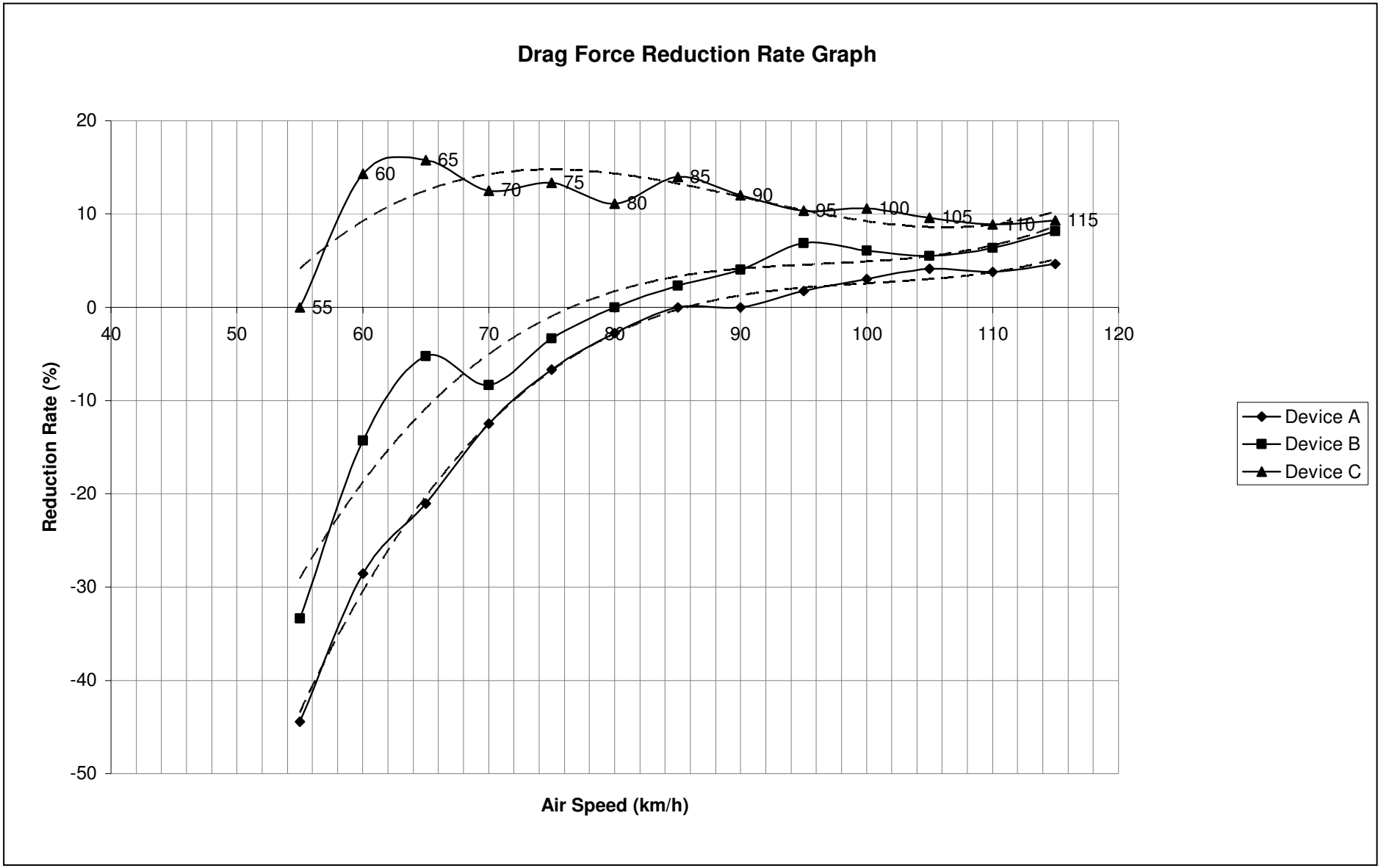

Figure 7.3. Reduction rate of drag force with air speed

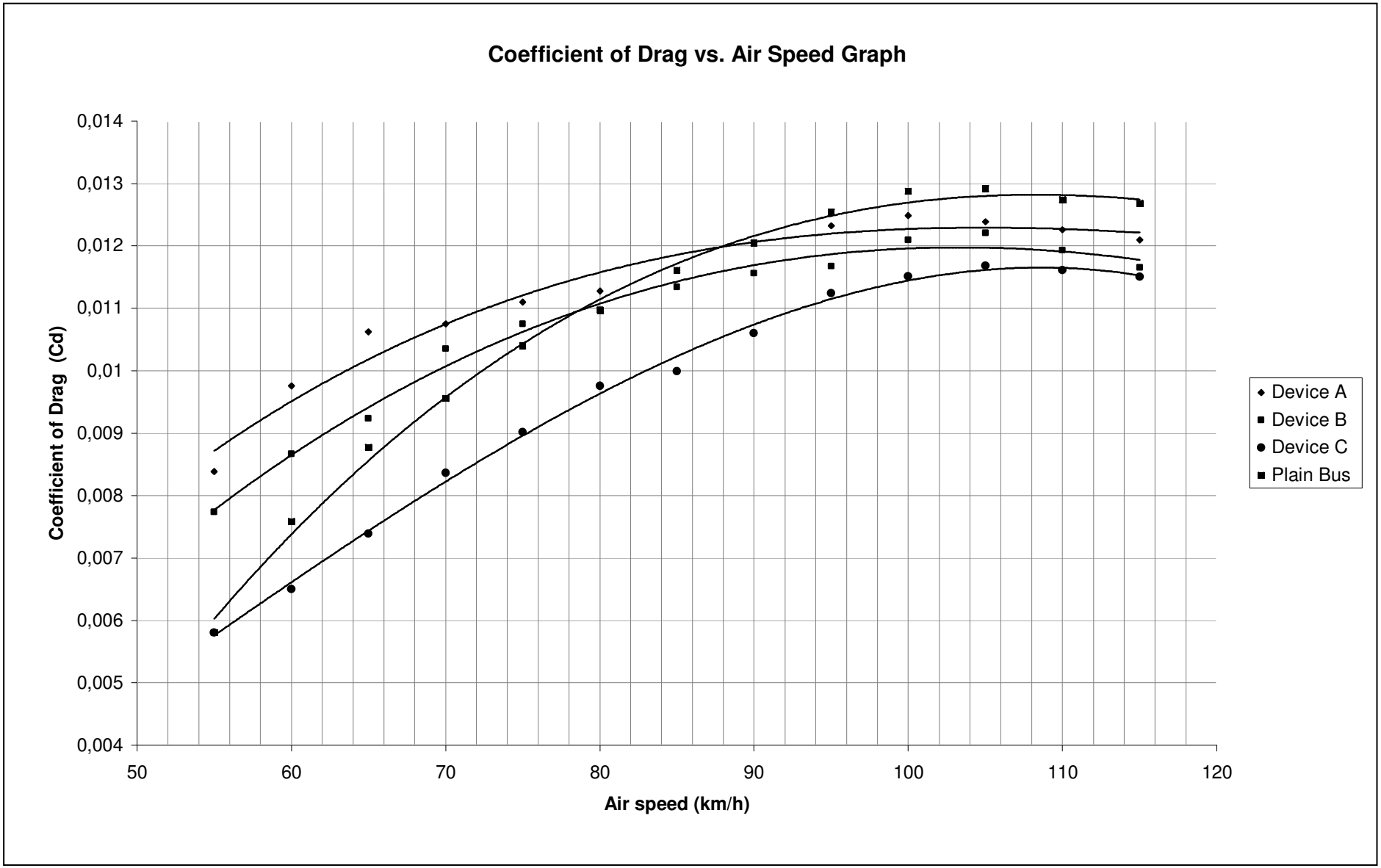

Figure 7.4. Coefficient of drag values at each speed level

As it can be clearly seen from the test results, the flow around the bus is changing when the devices are attached to it. At lower speeds it is noticed that the plain bus achieves less drag force than the other two devices but as the air speed increases, the results change as expected (Fig. 7.1). That is, the drag force acting on the plain bus is greater then the device attached cases. The unexpected situation at the lower speeds is arising from measurement and other system errors. This can be also better seen in Figure 7.2, which shows the reduction in drag force. As it can be seen for the devices B and C, the graph starts from the negative region, which means that they increase the drag force. However at higher speeds, more specifically after 90 km/h, they turn to reduce the drag force and show positive performance. On the other hand device C already starts in the positive region and it decreases the drag force up to 0.08N. In the plot, the fitting curves are also seen, which are polynomial functions of the third order. It can be seen from Table 7.2 the equations of these fitting curves and the R^2. They show that these fitting curves greatly represent the data, since they are very close to 1.

Table 7.2. Equations of the fitting curves for reduction in drag force

	Equations of the Fitting Curves	R^2
Device A	y = -4E-07x3 + 0,0001x2 - 0,0084x + 0,141	0,9885
Device B	y = -3E-07x3 + 7E-05x2 - 0,0054x + 0,0868	0,9650
Device C	y = 2E-07x3 - 7E-05x2 + 0,0084x - 0,277	0,9670

In Figure 7.3, the reduction rate in drag force due to the devices can be seen and the equations of the fitting curves and the R^2 values are represented in Table 7.3. The plot shows that the reduction rate settles around 8-9% at the highest speeds.

Table 7.3. Equations of the fitting curves for reduction rate in drag force

	Equations of the Fitting Curves	R^2
Device A	y = 0,0005x3 - 0,1369x2 + 13,815x - 464,88	0,9968
Device B	y = 0,0004x3 - 0,1273x2 + 12,329x - 395,33	0,9399
Device C	y = 0,0004x3 - 0,109x2 + 9,5826x - 259,88	0,5992

The change in the coefficient of drag values and the corresponding fitting functions are represented in Figure 7.4 and Table 7.4. They show that the Cd values change with the air speed.

Table 7.4. Equations of the fitting curves for Cd values

	Equations of the Fitting Curves	R^2
Device A	y = 1E-08x3 - 4E-06x2 + 0,0006x - 0,0102	0,9654
Device B	y = 6E-09x3 - 3E-06x2 + 0,0005x - 0,0106	0,9878
Device C	y = -2E-08x3 + 2E-06x2 + 5E-05x - 0,0017	0,9970
Plain Bus	y = 1E-08x3 - 6E-06x2 + 0,0008x - 0,0229	0,9960

Normally, the Cd values should be the same at each speed level, since it is a constant value. This reason for these changing Cd values is that, the Reynolds numbers were not matched inside the wind tunnel. Therefore the Cd values changed during the tests. However, it should be noticed that the Cd values are becoming close to each other as the air speed increases. This is occurring because of the nature of bluff bodies. Since a bus is also a bluff body, the coefficient of drag becomes constant after some point. The fitting curves also show that their slope becomes smaller. That is, the drag force acting on the plain bus is greater then the device attached cases. The unexpected situation at the lower speeds is arising from measurement and other system errors.

The wind tunnel results showed that placing the devices at the front of the bus has positive effects on reducing the drag force. It was expected to have such an improvement in drag force reduction. Especially the third device, that is the device C, which was selected as the most efficient design in the computer simulation, showed also in the tunnel tests the best reduction rate. The drag force reduction rates of the devices after the point all devices produce positive reduction rate, are listed in below table.

Table 7.5. Drag force reduction rates

Device Type	Drag Force Reduction Rate (after 85 km/h)
Device A	2,5%
Device B	5,6%
Device C	10,7%

It is seen that the third device has achieved a reduction in drag force of about 11%. This amount of reduction is very close to the results of the computer simulation, which was 12%. This shows that the wind tunnel data almost coincides with the computer simulation results.

CHAPTER 8

CONCLUSION AND FUTURE WORKS

In this research project, it was investigated what effect a drag reducing device applied on the front of a bus, has in terms of drag force reduction. Study showed that by only reducing the front drag, the overall drag force can be reduced. As opposed to other passive drag reduction devices, a mechatronic system was designed as a drag reducer. Initially the drag reduction device is simulated totally in the computer environment. The fluid dynamics simulation of the device under different flow conditions has been investigated and an efficient device shape is determined. Afterwards, to validate the simulation results and observe the real flow condition, a small low speed wind tunnel has been constructed. Testing three different devices in the wind tunnel showed that they have an effect on the drag force. Wind tunnel test results showed that the different geometrical shapes of the devices have different effect on the air flow, and thus cause different amounts of drag force reduction. Test results for the tested three devices showed a reduction in drag force as 3%, 8% and 11%. These results indicate that the mechatronic drag reduction device can have important effects on the drag force reduction and fuel savings in busses.

In the first chapter it was seen that a lot of research has been done on drag force reduction and all of them have reported different amount of success. The next step in drag reduction research should be combining different drag reduction devices into one system.

This project can be carried on by modifying this design to trucks and tractor trailers. In this way, the drag reduction device will be applicable to more vehicles and from economic point of view; a bigger success can be achieved. Looking at the mechatronic drag force reduction concept, from a very different point of view, it can be suggested that this concept might be useful for tall buildings and skyscrapers, where at high stages the air streams become important. A device, in a similar concept, attached on to a building could reduce the drag force on the building in high wind speed situations.

The mechatronic drag reduction device is designed for the reduction of the front drag. However, the base drag occurring at the back of the vehicle has also major effects on the total drag. Therefore an improved design which deals with both the front and base drag can be investigated. In order to achieve the base drag reduction, a mechatronic device acting like base plates can be designed and attached at the back of the vehicle. In such a combination of devices, the air flow around the vehicle will be more under control, which means less turbulence and less drag force.

Another research direction can be the treatment of the underbody of heavy vehicles. An important problem in tractors and trucks is that the gap between the vehicle and the ground is relatively high when compared with busses. During the trip, airflow enters the underbody and increases the drag force. This problem can be solved by designing a mechatronic system, which covers the sides of the vehicle and prevents the air from flowing in. In this way the wheels of the vehicle can be also enclosed with the mechatronic system. Simply, the mechatronic system will work as a curtain, which opens and closes, during the trip.

In conclusion, success in drag force reduction can have a very big impact on transportation. Small improvements in the fuel efficiency of heavy duty vehicles and busses can turn into significant amounts of fuel savings. This in turn would have an important effect on the total economy. When looking from this point of view, it can be realized that newer research in drag force reduction could bring important advantages to the transportation arena.

REFERENCES

Bauer, S. and Wood, R., "Base Passive Porosity for Drag Reduction", United States Patent 6,286,892, Sept. 11.2001

Bauer S. and Wood R., Base Passive Porosity for Drag Reduction, United States Patent 6, 286, 892, Sept. 11, 2001

Bearmann, P.W., Investigation of the Flow behind a Two Dimensional Model with Blunt Trailing Edge and Fitted with Splitter Plates. J.Fluid Mechanics, Vol. 21, 1965, pp.241-255

Bearmann, P.W., Investigation into the effects of Base Bleed on the Flow behind a Two Dimensional Model with a Blunt Trailing Edge. AGARD Conf. Proc., No. 4, Separated Flows, Part 2, 1966, pp 479-507

Englar, R.J., "Advanced Aerodynamic Devices to Improve the Performance, Economics, Handling and Safety of Heavy Vehicels", 2001-01-2072, SAE Government/Industry Meeting, May 14-16, 2001

Kruppa, E.W., A Wind Tunnel Investigation of the Kasper Vortex Concept AIAA 77-310, Jan. 10-13, 1977

Mason, W.T.Jr. and Bebe, P.S., "Drag Related Flow Field Characteristics of Trucks and Busses", Plenum Press 1978

Mode, V.J. and Deshponde, V.S., "Aerodynamics of Building with Momentum Injection", AIAA, 2001-2456

Rae Jr., William H. and Pope, Alan. Low-Speed Wind Tunnel Testing. New York, Wiley & Sons, 1984

Wood, R.M., 2004 “Impact of Advanced Aerodynamic Technology on Transportation Energy Consumption”, 2004-01-1306

Wood, R.M. and Bauer, S.X.S., “Simple and Low Cost Aerodynamic Drag Reduction Devices for Tractor-Trailer Trucks”, 2003-01-3377, November 2003

Web_1, 2005. AirTab website, 2005, http://www.airtab.com

Web_2, 2005. Aerodyn website, 2005, http://www.aerodyn.org/Drag/tables.htm

Web_3, 2005. Aerodinamik web sitesi, 2005, http://www.e-scoot.com/2000/hul/aerodynamics.htm

Web_4, 2005. Simtec website, 2005, http://www.simtec.ch/index.php?option=content&task=view&id=36&Itemid=68&PHPSESSID=a96608be5225d245eea2a5b4429e4ef1

Web_5, 2005. PadokF1 website, 2005, http://www.padokf1.com/dosya/63

Web_6, 2005. ASE website, 2005, http://www.aerosysengr.com/Wind_Tunnels/WTProducts/Flow_Conditioning/flow_conditioning.html

Web_7, 2005. Explorer Yachts’ website, 2005, http://www.buyexploreryachts.com/expeditionyacht-news-bulb.html

Web_8, 2005. Cepolina’s website, 2005, http://www.cepolina.com/freephoto/va/airplane-object.htm

Web_9, 2006. Aerosys’ website, 2006, http://www.aerosysengr.com/Wind_Tunnels/WTProducts/Flow_Conditioning/flow_conditioning.html

APPENDIX A

EQUATION CONSTANTS OF THE 2D CURVES

$$y(x) = ax^{10} + bx^{9} + cx^{8} + dx^{7} + ex^{6} + fx^{5} + gx^{4} + hx^{3} + ix^{2} + jx + k$$

	1	2	3
a	-1,40534539215375E-25	-6,99773191329921E-26	6,65812915415760E-25
b	9,94998126802744E-22	4,84375877245302E-22	-3,90279686497418E-21
c	-3,06256432416883E-18	-1,44949434040106E-18	9,62769684849071E-18
d	5,37359518844703E-15	2,46023205869615E-15	-1,29555563189788E-14
e	-5,92006166823590E-12	-2,61438738329730E-12	1,02583916856241E-11
f	4,24951203362301E-09	1,81528614724480E-09	-4,74155116189202E-09
g	-1,99561643669828E-06	-8,38029784905916E-07	1,12198444862505E-06
h	6,00212175668062E-04	2,59486471683356E-04	-3,97638102568671E-05
i	-1,11066657494011E-01	-5,53584372328490E-02	-4,38747201811742E-02
j	11,95132158743	8,29827389339269	10,2597613900575
k	1,01854769561967E-03	1,73273416878128E-02	8,29150996274857E-02

	4	5	6
a	-6,37116230064170E-26	-9,53088724811969E-26	-1,73895668479268E-26
b	4,46177621564911E-22	6,66649689617561E-22	1,19220942212895E-22
c	-1,35558206948189E-18	-2,02214175076168E-18	-3,58696855392731E-19
d	2,34677147913984E-15	3,49132299679159E-15	6,29727707430116E-16
e	-2,55905169515651E-12	-3,78851227076187E-12	-7,27114047131429E-13
f	1,83814398426579E-09	2,69609227014050E-09	5,92389216355748E-10
g	-8,87743146474176E-07	-1,27902571056171E-06	-3,55679533746278E-07
h	2,91991096398279E-04	4,06631983970680E-04	1,59592258504626E-04
i	-6,70595966039148E-02	-8,79033043786645E-02	-5,24387258822675E-02
j	10,6039768811366	12,7670857210645	10,9508220307748
k	6,54070471876524E-03	9,01517358942769E-03	2,36147450430986E-03

	7	8	9
a	1,34394050493312E-25	1,08370356222471E-25	1,98083807799831E-25
b	-9,35770692627377E-22	-7,60980951347334E-22	-1,37360540281631E-21
c	2,80776628583208E-18	2,30279133810263E-18	4,10835597827636E-18
d	-4,73841686776784E-15	-3,91815953236423E-15	-6,92169641413158E-15
e	4,91372978611321E-12	4,09172636321310E-12	7,18471547566566E-12
f	-3,19606103404341E-09	-2,67083890283670E-09	-4,70175230249814E-09
g	1,25674648412853E-06	1,04231552443770E-06	1,88312970038799E-06
h	-2,52926525963325E-04	-1,97438353276255E-04	-4,04064094969398E-04
i	2,39838680540150E-03	-7,11533562336214E-03	1,81168131223705E-02
j	8,6776262274357	9,9013000964824	9,3147236586731
k	-1,17162952165434E-02	-9,08317771952424E-03	-1,58693248459995E-02

	10	11	12
a	1,26646250287409E-25	-2,27363760633644E-25	2,94678417101154E-25
b	-8,87778209108963E-22	1,26488179740777E-21	-2,05578687504103E-21
c	2,68035036478176E-18	-2,85656071695737E-18	6,18318762426199E-18
d	-4,54635507797434E-15	3,29497803688950E-15	-1,04732695282538E-14
e	4,72643161946719E-12	-1,93538027636335E-12	1,09327759204704E-11
f	-3,06322662697095E-09	3,99471436750234E-10	-7,20713401749308E-09
g	1,17943662771534E-06	1,06744398669290E-07	2,92531371632042E-06
h	-2,14608672086150E-04	-3,10490144902836E-05	-6,52526899307047E-04
i	-1,22200907780952E-02	-2,81096478597611E-02	4,30274752224175E-02
j	11,9531418711739	12,9965602297075	10,4213047143927
k	-1,10245562763070E-02	-5,45356770825832E-02	-2,74679879311419E-02

	13
a	3,41725152926695E-25
b	-2,37880883943359E-21
c	7,13595695943066E-18
d	-1,20486821912985E-14
e	1,25286274655294E-11
f	-8,21979999651725E-09
g	3,31641132885069E-06
h	-7,34229611613212E-04
i	4,81317551585442E-02
j	11,4241597545403
k	-3,29053963831731E-02

APPENDIX B

EQUATION CONSTANTS OF THE 3D SHAPES

$$y(x) = ax^{10} + bx^{9} + cx^{8} + dx^{7} + ex^{6} + fx^{5} + gx^{4} + hx^{3} + ix^{2} + jx + k$$

	Extrusion Curve (8,5%)
a	-1,08673554464251E-24
b	6,76662800070080E-21
c	-1,81418737416540E-17
d	2,74119182665908E-14
e	-2,56586335503994E-11
f	1,54090978203979E-08
g	-5,95209802937551E-06
h	1,44647528134323E-03
i	-2,12001725993415E-01
j	17,40728256805380
k	0,86056226830359

	Cut Curve (8.5%)
a	-2,71823059605449E-28
b	3,32992186637645E-24
c	-1,78240194249921E-20
d	5,47477606551021E-17
e	-1,06562956735571E-13
f	1,36957293925969E-10
g	-1,17525555452718E-07
h	6,67448475703154E-05
i	-2,44957487989376E-02
j	5,55710739671287
k	0,16009196843718

Extrusion Curve (10,2%)	
a	-3,28647907106386E-25
b	1,99352153446352E-21
c	-5,18220425005290E-18
d	7,54436094949344E-15
e	-6,75163177201373E-12
f	3,84655278282194E-09
g	-1,40782387205793E-06
h	3,34087020123503E-04
i	-5,46976039720778E-02
j	6,68666761677826
k	0,35861476829042

Cut Curve (10,2%)	
a	-5,03460983567601E-28
b	6,16667990366200E-24
c	-3,24689282574071E-20
d	9,61176242533786E-17
e	-1,75815293630692E-13
f	2,05990495733793E-10
g	-1,55615091529928E-07
h	7,51102530810894E-05
i	-2,29392218957108E-02
j	4,42658855167444
k	0,28544149737463

Extrusion Curve (12%)	
a	2,27274594089769E-25
b	-1,38865993735889E-21
c	3,60929993846428E-18
d	-5,20270736475936E-15
e	4,54565996781255E-12
f	-2,46434112428839E-09
g	8,05082830726229E-07
h	-1,37550291021924E-04
i	2,42173717094038E-03
j	3,70778382054542
k	-0,19018406390805

Cut Curve (12%)	
a	-3,10286114928942E-28
b	3,79124204844572E-24
c	-2,01275737841895E-20
d	6,09171453997543E-17
e	-1,15885225089408E-13
f	1,44005142543513E-10
g	-1,17691589074997E-07
h	6,23109049914090E-05
i	-2,08294367671619E-02
j	4,38245417424267
k	0,30834253888755

APPENDIX C

SOLIDWORKS® AND COSMOS FLOWORKS®

The design of the mechatronic drag reduction device was entirely made in SolidWorks. The three dimensional model of the bus and the mechanism of the device is simulated inside Solidworks (Fig. A.1). Then the fluid dynamics analysis of the model is made in Cosmos FloWorks (Fig. A.2).

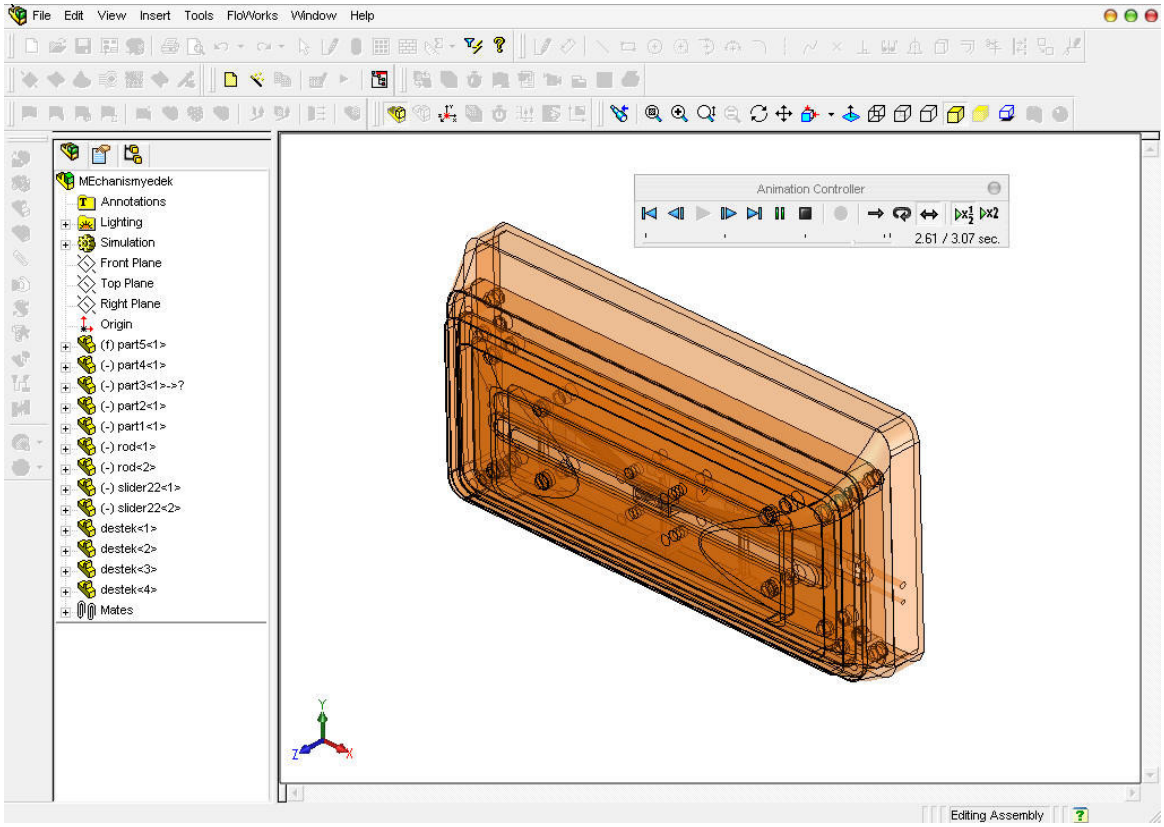

Figure C.1. Mechanism design in SolidWorks

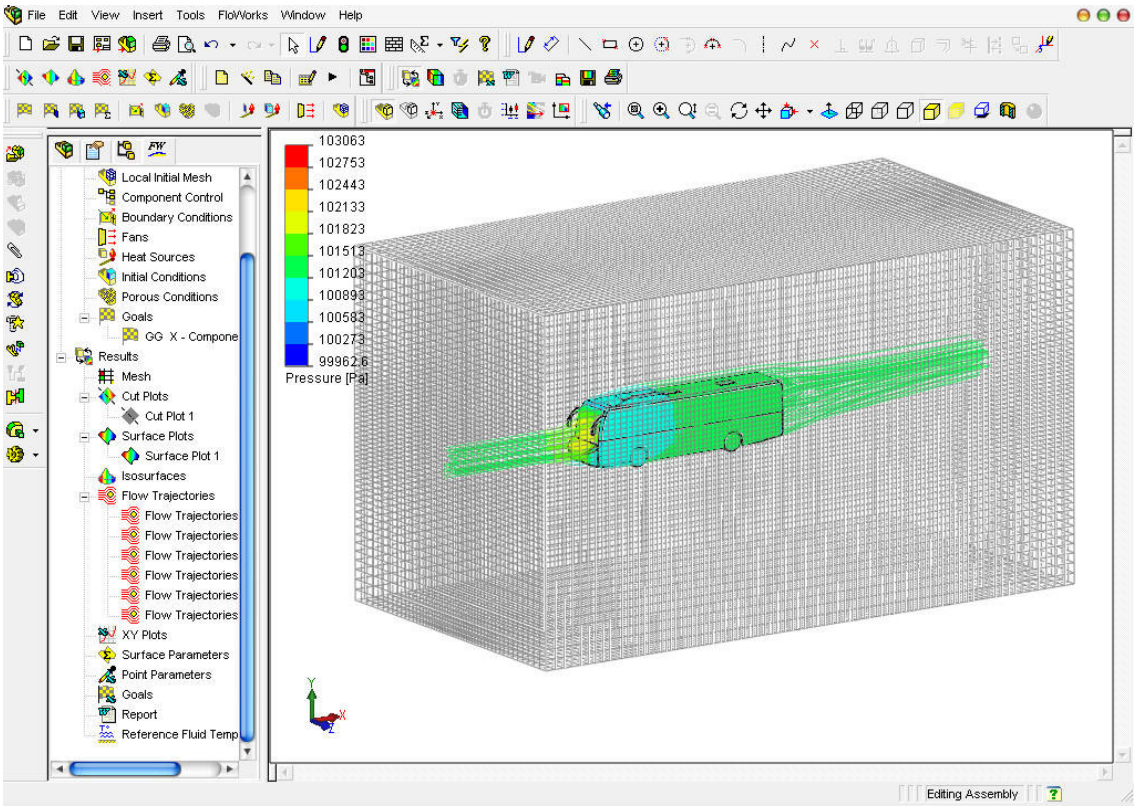

Figure C.2. Flow simulation in Cosmos FloWorks

APPENDIX D

STRENGTH ANALYSIS

The strength analysis of the links used in the mechatronic drag reduction device is made by using CosmosXpress, which is a static strength analysis tool for SolidWorks. The links are tested under varying load conditions and modified according to the analysis results. Below figures show how the links may deform under excessive loads.

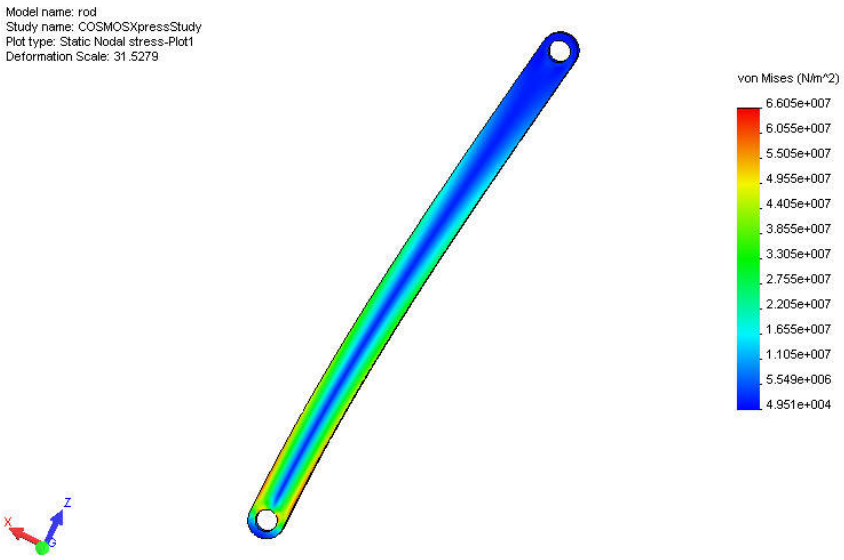

Figure D.1. Deformed shape of link

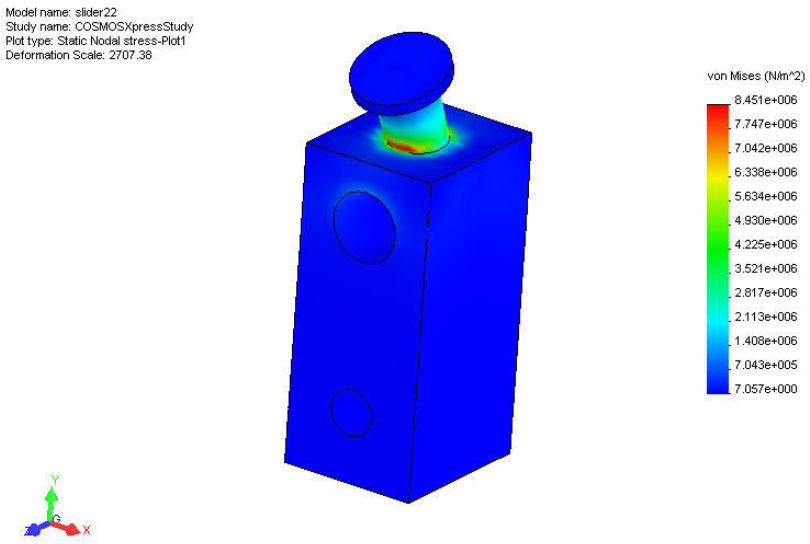

Figure D.2. Deformed shape of slider